SECURITY CLASSIFICATION OF THIS PAGE (When Data Entered)

REPORT DOCUMENTATION PAGE

READ INSTRUCTIONS BEFORE COMPLETING FORM

REPORT NUMBER	2. GOVT ACCESSION NO. AD-A157 632
3. RECIPIENT'S CATALOG NUMBER	
TITLE (and Subtitle) RESEARCH IN MATERIALS SCIENCE; Superconducting Transition Metal Alloys.	5. TYPE OF REPORT & PERIOD COVERED End of Contract Report June 1, 1973 -- May 31, 1975
	6. PERFORMING ORG. REPORT NUMBER
AUTHOR(s) R. M. Rose, M. L. A. MacVicar, J. L. Bostock	8. CONTRACT OR GRANT NUMBER(s) DAHC-15-73-C-0316
PERFORMING ORGANIZATION NAME AND ADDRESS Center for Materials Science and Engineering, Massachusetts Institute of Technology Cambridge, Mass. 02139	10. PROGRAM ELEMENT, PROJECT, TASK AREA & WORK UNIT NUMBERS
11. CONTROLLING OFFICE NAME AND ADDRESS	12. REPORT DATE July 31, 1975
	13. NUMBER OF PAGES
14. MONITORING AGENCY NAME & ADDRESS(if different from Controlling Office)	15. SECURITY CLASS. (of this report)
	15a. DECLASSIFICATION/DOWNGRADING SCHEDULE

16. DISTRIBUTION STATEMENT (of this Report)

APPROVED FOR PUBLIC RELEASE;
DISTRIBUTION IS UNLIMITED (A)

17. DISTRIBUTION STATEMENT (of the abstract entered in Block 20, if different from Report)

18. SUPPLEMENTARY NOTES

19. KEY WORDS (Continue on reverse side if necessary and identify by block number)

A15 compounds	$Nb_3(Al,Ge)$	amorphous carbon
superconductivity	Nb_3Al	Nb
tunneling	Nb_3Sn	β-W alloys
microwave cavities	junction barriers	transition metal alloys
Mo-Re	artificial barriers	transition metal oxidation

niobium, aluminum, germanium

20. ABSTRACT (Continue on reverse side if necessary and identify by block number)

Good superconductive tunneling has been obtained into $Nb_3(Al,Ge)$ ribbon substrates and sputtered films. Unfortunately, the data is surface limited and represents a disturbed layer of T_c<7K. Arc melted buttons of $Nb_3(Al,Ge)$ used as junction substrates have derivative curves which are reminiscent of deformed Nb tunneling data and are, therefore, difficult to interpret. Nb_3Sn substrates formed by the diffusion of Sn into Nb single crystals yield reproducible junctions with gap values ~3.6 mV; the tunneling characteristics are, however, not ideal. A systematic study of the electronic behavior of arc-evaporated amor-

about 1/4

DD FORM 1 JAN 73 1473 EDITION OF 1 NOV 65 IS OBSOLETE S/N 0102-014-6601

Block 19

deformed surface layers	tunnel junction deconvolution
X-band cavities	single crystal Nb
surface impedance	deformed Nb
numerical analysis	oxypolishing technique

Block 20

phous carbon films as a function of deposition rate, vacuum pressure, film thickness, ageing, and annealing was completed. General fabrication and performance criteria for effective tunneling barriers between a variety of metal and alloy substrates have been established. Superconductive tunneling was observed with electron beam evaporated amorphous carbon barriers on tin, indium, lead-impregnated porous glass, and bulk $Nb_3(Al,Ge)$. Using a $Mo_{.75}Re_{.25}$ alloy endplate on an X-band Nb cavity, an upper bound for the Mo-Re residual surface resistence was found to be 2.8 μΩ and a lower bound for the breakdown field 102 G. Initial tests with an entire Mo-Re cavity indicated unloaded Q-values of 5×10^7 - 1×10^9. Subsequent electropolishing and annealing reduced these Q-values to less than 10^7. Ongoing studies indicate alloy segregation and slowly-forming surface oxides as the cause of the cavity degradation.

EoR
(noted) file

END OF CONTRACT REPORT

Period: June 1, 1973 -- May 31, 1975

Title: Research in Materials Sciences

Project Title: Superconducting Transition Metal Alloys

Contract Number: DAHC 15-73-C-0316

ARPA Order Number: 2469

Program Code Number: 3D10

Name of Contractor: Massachusetts Institute of Technology
Cambridge, Mass. 02139

Principal Investigator: N.J. Grant (617) 253-5638

Project Scientists or Engineers: R.M. Rose (617) 253-3230

M. L. A. MacVicar (617) 253-6261

J.L. Bostock (617) 253-7607

Effective Date of Contract: June 1, 1973

Contract Expiration Date: May 31, 1975

Amount of Contract: $770,233

Amount of Project: $223,834

Sponsored By

Advanced Research Projects Agency

ARPA Order No. 2469

TABLE OF CONTENTS

VI. SUMMARY

This project has two main objectives: to unravel the complex problem of superconductivity of high T_c A15 materials by tunneling experiments and to develop materials for practical superconducting microwave cavities. The blueprint for this research is as follows: the digital hardware and software for processing of tunnel data is to be improved and expanded in capability; tunneling experiments on the surfaces of A15 compounds prepared in a planned manner will be performed; the feasibility of using various artificial barriers on the A15 substrates will be determined; and, relative microwave losses at X-band for a variety of materials and surface treatments will be determined by using a cavity with a removable back-plate. In this report we describe our progress towards these goals achieved in the first two years of this research.

(a) To extract the basic parameters for A15 superconductivity by tunneling techniques:

In the initial stages of the contract we were able to obtain good superconductive tunneling into $Nb_3(AlGe)$ ribbon substrates and sputtered films. Although these A15 samples offer good flat surfaces for barrier formation and thus a high probability for successful tunneling, they were inhomogeneous and surface limited resulting in effective tunneling T_c's less than approximately 7K.

Arc melted $Nb_3(AlGe)$ buttons, fractured to reveal interior surfaces and subsequently mechanically or chemically polished, were also used as junction substrates. All of these A15 samples contained at least a small

percentage of second phase material and exhibited a fair amount of porosity. Their tunnel junctions were characterized by high leakage currents and large normal current backgrounds. The first derivative data which is reminiscent of deformed Nb tunneling data, is, therefore, extremely difficult to interpret. One or two of these junctions did, on the other hand, have reasonably good derivative curves consistent with energy gaps ∿2mV. One arc melted Nb_3Al sample with an observable Al-depleted surface layer also exhibited a clean first derivative. The corresponding gap-ratio ($2\Delta/kT_c$) is ∿3.2 which is very BCS-like. In the arc melted samples there is a definite improvement of tunneling characteristics with increasing perfection of the sample surface.

Tunneling into Nb_3Sn has also been achieved. The Nb_3Sn samples are obtained by diffusion of Sn into single crystals of Nb. Natural oxide barriers are then fabricated by oxypolishing the surface of these cylinders and subsequently immersing the specimens in an atmosphere of pure oxygen for 20 to 30 hours. Junctions fabricated in this manner are not only often of good quality but yield data which is reproducible from junction to junction. The barriers are also quite stable and able to withstand repeated recycling to room temperature. Typical energy gap values appear to be on the order of 3.6 mV which gives a gap ratio ∿5.2. If our interpretation of the data is correct, this is the strongest coupled material that has ever been observed. Recently with the improvement of our tunneling characteristics we have been able to see the image of the lead counter-electrode phonon spectrum in the derivative curves; it is accompanied by other apparent phonon structure which we believe is due to the A15 substrate.

The tunneling data deconvolution software which extracts the phonon spectra and electronic density of states of unknown junction components has been implemented and debugged. These computer programs enable us to look at any combination of tunneling electrodes, even those with strong coupled superconductors on both sides of the barrier. (In the latter case, the phonon spectrum of one side must be known.) The programming has been used successfully to extract the phonon spectrum of Nb from both single crystal and deformed Nb junctions with three different counter-electrodes: Au, In, and Pb.

One implication of the above is that we can look, with greater precision than we thought possible, at more kinds of junctions than we thought possible. The initial success at tunnel junction fabrication on various kinds of A15 substrates and the improving tunnel characteristics with improved substrate surfaces indicate that the goal of this research is definitely feasible, and we continue to tackle the substrate surface problem with optimism.

(b) To develop appropriate artificial barriers for A15 tunnel junction substrates:

A systematic study of the electronic behavior of arc-evaporated amorphous carbon films was completed. Rates of evaporation from 2 Å/sec to 150 Å/sec, vacuum pressures varying over three decades, and thicknesses of ~50 Å to over 1000 Å were investigated. Resistivity was typically 1Ω-cm for films deposited at rates >10Å/sec in 10^{-5} T vacuum at >100 Å thickness. A slower rate yielded markedly different, non-predictable resistivity values.

Electron microscope studies showed all as-grown films to be amorphous on a scale of 2Å. Temperature dependence of the resistivity was investigated over the range 4.2°K to 500°K; generally, log ρ followed a $T^{-\frac{1}{4}}$ behavior. Activation energies of the carbon film gap values at liquid helium temperatures were estimated as 3 to 5 meV. This range of values is sufficient as a barrier height betwen superconducting electrodes applied to the carbon films to form S-C-S' tunneling sandwich configurations.

Extensive investigation of electron-beam fabricated amorphous carbon films were also undertaken. In particular a general set of criteria for depositing usable carbon film barriers has been established in terms of deposition rate, film resistivity, and film color. These criteria seem generally applicable to both arc-evaporated and electron-beam fabricated carbon films. Superconductive tunneling was observed from a variety of different junctions with electron-beam evaporated amorphous carbon barriers: tin, indium, lead-impregnated porous glass, bulk $Nb_3(AlGe)$.

The implications of this study are that as long as sufficient care is taken in the carbon barrier fabrication (and, of course, that intermetallic compounds or diffusion layers do not form), these films can be used as insulating layers in junctions where the substrate oxidizes poorly or has conducting oxides. The major cases in point are V and the V-alloys, especially the A15 V-compounds V_3Si and V_3Au. Once the problems encountered in perfecting a representative surface in these materials have been overcome, carbon barriers will be needed to fabricate superconductive tunnel junctions.

(c) To develop improved surfaces, materials, and surface treatments for superconducting microwave devices:

By using a $Mo_{.75}Re_{.25}$ alloy endplate on a Nb microwave cavity (TE_{011} mode, resonant at 11.2 GHz), an upper bound for the residual surface resistance of this alloy was shown to be 2.8 μ-Ω and a lower bound for the breakdown field, 102 G. No particular effort was devoted to optimization of the surface quality of this backplate. Since the corresponding surface resistances at lower frequencies would therefore be well within the range required for practical devices, and the surface condition appeared to be much less critical than that of Nb, two cavities entirely of Mo-25Re were constructed. Preliminary tests were encouraging (residual unloaded Q's of 5×10^7 -1 X 10^9) but subsequent treating and testing suggest that alloy segregation (probably due to impurity contamination) and slowly-forming surface oxides may be degrading Q.

The Mo-Re cavities were delivered to us in June of 1974 and January of 1975 so that we are still in the preliminary stages of preparing and testing them. Thus, since the problems we are encountering are the main thrust of this aspect of our proposed research, we are neither surprised nor discouraged that, at this time, they are non-trivial. There are not, we believe, any long term implications in our present situation.

I. INTRODUCTION

The original premise of this research is the vital importance of a fundamental understanding of transition metal superconductivity with a particular emphasis on compounds with the A15 crystal structure. The two central goals are to determine the basic parameters governing the high temperature superconductivity of A15 materials and to develop improved surfaces, materials, and surface treatments which will make superconducting microwave cavities practicable.

Although many theories have been proposed, no one today understands why A15 compounds form the class of highest transition temperature superconductors. Considering the impact that raising the maximum T_c to $\geq$25K* would have on the technology of generation, conversion, transmission, and utilization of energy, it is important to find out the essential ingredients for making high T_c materials. Many of the basic microscopic parameters of the A15 compounds have yet to be determined: the pairing potential, the density of states, the phonon spectrum, the energy gap, and any anisotropies or anomalies in these parameters particularly as they relate to the metallurgical history of the sample. Obtaining this data is necessary before any effective use of the existing theoretical predictions for increased T_c materials can be made.

The method of electron tunneling is a particularly powerful way of

---

*In the liquid neon range.

obtaining such information as long as the inherent surface and metallurgical problems characteristic of these materials can be solved. Sufficiently high quality tunneling data will enable us to extract directly the electron-coupled phonon spectrum and all the other microscopic parameters which are necessary for a description of A15 superconductivity in terms of strong coupling theory.

The other central goal of this research is to develop the technology for the manufacture of practical superconducting microwave cavities and similar devices. The application of superconductivity to microwave technology (in particular, the S, L, and X bands) has demonstrated that very large quantities of power may be handled with unprecedented efficiency; in the X-band, quality factors in excess of 10^{11} have been attained with frequency stability exceeding that of the best quartz crystal systems. The only area where the potential advantages have been extensively explored and calculated however, is in high energy physics, where the use of superconducting microwave cavities affords a number of striking technical advantages over the corresponding conventional devices, most of them associated with the huge quality factors attainable (10^{11} or more) and high rf fields (well above 1 kOe). The extreme stability of such cavities has also made possible, for example, the development of superconducting-cavity-stabilized microwave oscillators with remarkable properties. There are undoubtedly many other potenial applications such as high field rf plasma containment devices, but all such must await the development of a reliable, economical fabrication technology, which can consistently produce superior cavities whose properties will not degrade

with time or exposure to relatively benign atmospheres.

In the present research the experimental obstacles to obtaining detailed information on the surface and bulk properties of both the A15 compounds and other transition metal alloys are basically identical: one must prepare a smooth, clean surface, whose properties are representative of the interior of the superconductor, and on top of the surface, the thin oxide film which forms must be continuous, homogeneous, smooth and (at cryogenic temperatures) a reasonable insulator. On the other hand, the potential end results of the research are also non-trivial:

(1) substantial advancement of our understanding of superconductivity of the A15 compounds and the origins of high transition temperatures in these materials;

(2) new understanding of the nature of the surfaces of transition metal alloys and compounds;

(3) new and better methods for the manufacture of superconducting microwave devices.

In this report we discuss at some length the three different aspects of our research to date. The first section contains a description and analysis of the tunneling data we have obtained from various A15-substrate junctions (mainly having natural oxide barriers). The methods of surface preparation and barrier fabrication are extensively reviewed here. Nb_3Sn samples, made by diffusing Sn into a Nb single crystal are the most promising in terms of observing the phonon structures of both the A15 compound and the junction counter-electrode in the first derivative tunneling

curves. In this section we also report briefly on the progress made with the numerical analysis techniques for extracting phonon information from superconductive tunnel data. (This has been done in conjunction with another project, sponsored by ONR.)

The second section details our approach toward determining the connection between final tunneling barrier quality and the fabrication parameters of thin amorphous carbon films (e.g., deposition rate, thickness, pressure, and substrate species). The electronic behavior of arc-evaporated carbon films indicates that these films, acting as insulative layers in tunnel junctions, should have sufficient activations energies to make them useful barrier materials. The behavior of electron-beam deposited films as the barrier element in a metal-carbon-metal sandwich configurtion for various substrate species is described in detail. General criteria for the successful fabrication of carbon barriers in tunnel junctions are discussed. These criteria establish rather narrow parameter limits outside of which some very undesirable effects from the point of view of superconductive tunneling come into play.

In the third and final section the progress we have made on the feasibility of using Mo-25Re in superconducting microwave devices is outlined. The initial trials using a Mo-Re back-plate on a solid Nb cavity which indicated that even without extensive preparation of the Mo-Re surface, this bcc alloy might well meet or surpass the standards required in X-band cavity work are reviewed. A complete discussion of the fabrication and testing parameters for two removable backplate cavities made entirely of Mo-Re is presented and the results of the characterization of our surfaces is

given. We believe that our present problems revolve about the continuous formation of oxides on the cavity surfaces as a function of sequential annealing for the various trails.

II. Tunneling into A15 Compounds

Attempts at tunneling into A15 compounds have thus far met with little real success, due not only to metal processing difficulties, as in other transition metal series, but to the capriciousness of the oxide barrier fabrication. Beyond the requirement that the tunnel barrier must be continuous, uniform, and insulating, an additional problem arises for superconductors of extremely short coherence length: the interface region (the transition region from barrier to bulk material) now constitutes a significant fraction of the region sampled by the tunneling electrons, even for interfaces which would ordinarily be considered quite sharp. In fact, the surfaces of A15 compounds as prepared by current methods are not sharp in any sense of the word, and, these alloys are known to have very short coherence lengths.[1] Hence, extreme caution must be taken in interpreting data from A15 junctions because it might reflect a surface limited condition unless means are devised to ensure truly representative properties near the surface.

Our approach to the actual tunneling into the A15 substrates is two-fold: a careful procedural development of different barrier fabrication processes on flat ribbons and sputtered films and (concurrently) an investigation of the suitability of various bulk samples as junction substrates including arc cast, annealed A15 button surfaces and diffusion layers of A15's on Nb single crystals. Early in this investigation we obtained good superconductive tunneling into the ribbon and film substrates with oxide tunnel barriers fabricated either thermally or by a glow discharge technique.[2] These junctions had a number of disadvantages: poor shelf

and cycling life, very low yield, and measured energy gap values well below what would be expected from the measured bulk transition temperature, i.e., $\Delta(0) \sim .2 - .4\ k_B T_c$. These problems were not unanticipated, and the two main problems were easily isolated: the fabrication of sound, stable tunneling barriers; and assuring that the layer of A15 substrate within a coherence distance of the barrier is representative of the bulk material. Structures related to both of these problems were readily observed in the junction I-V characteristic and its derivatives.[2] Further attempts to make these substrate surfaces more representative of the bulk resulted in decidedly poorer tunneling characteristics for both types of oxide barrier junctions.[3]

Subsequent investigations of the bulk A15 substrates indicated far more encouraging results at the early stages of junction fabrication. First, it appeared possible to remove the naturally occurring depleted surface layers; then, although naturally occurring oxides were fragile and unable to withstand either thermal or voltage cycling, various means of assisting oxide growth resulted in increased durability; and, as the substrate surface perfection increased, the tunneling data improved correspondingly. For the latter reason we have concentrated our most recent efforts on the bulk substrates: $Nb_3(AlGe)$ and Nb_3Sn.* We have made a systematic and extensive exploration of the various means of natural oxidation of their surfaces; e.g., thermal, glow discharge in oxygen partial pressures,

---

*The Nb_3Sn substrates are generated by equilibration of a Nb single crystal in a saturated Sn atmosphere.[4]

atmospheric, anodization, acid etching, and oxypolishing (or anodic stripping). Many of the above technqiues have resulted in identifiable superconducting tunnel characteristics, some even exhibiting phonon structure.

Although nearly ideal junctions will have to be obtained before phonon structure in the first derivative tunneling can be numerically processed, we are developing, in parallel, our phonon deconvolution programming. The results of this research may enable us to set-up guidelines and procedures for judging the extent to which the tunneling in A15's reflects true bulk properties or only partially removed, disturbed surface layers.

(i) Previously Reported Research

Early in the course of these investigations[5] commercial-type $Nb_3(AlGe)$ ribbons and rf sputtered films were chosen as substrate material since the existence and accessibility of flat surfaces in these geometries make them especially suitable for tunneling. The ribbons were fabricated by a process developed in this laboratory[6] and the films were sputtered from compacted and unreacted ribbon material.* X-ray diffraction and metallographic studies showed more than 90% of each sample possessed the A15 structure. Whereas the transition temperature of the films was always <7K, the ribbon substrates had midpoint transitions of 17.5K which increased to 19K on low temperature annealing (725C for 90 hours in

*These films were supplied by the IBM Thomas J. Watson Research Center

less than 10^{-5} Torr).

Of the nearly 70 junctions tested only 2 showed nearly ideal first derivative traces and only 9 yielded typical (identifiable) superconductive tunnel data. These include both carbon barrier and oxide barrier junctions. On the whole there was little difference in the quality of the two kinds of junctions. In all of the successful samples the substrate was first cleaned with a chemical etch* to remove the outside layers of the ribbon and, consequently, any depleted or cold worked layers at the sample surface (and remaining cupronickel tubing contaminants on the ribbons). This was followed by glow discharge cleaning.** Barrier layers included oxide layers formed either by anodization in a glow discharge system without exposure to atmosphere (the sample is held at a few hundred volts above the cathode in 5 X 10^{-2} Torr O_2)[7] or by placing the samples in a free flow of oxygen at 150C (called a thermal oxide), and amorphous carbon barriers prepared either by arc evaporating 150Å of carbon onto cleaned ribbon substrates or by electron beam depositing carbon films on both the $Nb_3(AlGe)$ ribbons and films.[1,5]

The results were not uniformly good: only two of these junctions had clear sharp gap structure and near ideal derivatives and even these had high excess currents. The rest showed either hysteresis or microshorts, overwhelming background current, barrier-related structure, and/or

---

*10:20:30 parts (HF, HNO_3, lactic acid).

**The sample was maintained at a negative potential difference greater than 1000V in 30 X 10^{-3} Torr of Argon.

inconsistent gap structure superimposed on the desired characteristic. In addition, all the junctions had fragile barriers that could not stand up to either temperature recycling or sustained bias.[2,5] Our best results were obtained with unannealed ribbon mounted as the anode in the argon discharge and on which a thermal oxide barrier was subsequently formed. The first derivative plot of one of these two junctions is shown in Fig. (1). [The temperature of 2.6 K of the lower trace is only approximate since the sample cooled by an additional 150 mK while the derivative was being scanned.[2]] The value of 2Δ for $Nb_3(AlGe)$ obtained from this junction is 0.7 meV at 4.2 K and 1.2 meV at 2.6 K. If the energy gap followed the empirically desired temperature dependence,[8] we would obtain $T_c = 4.6$ K and $2\Delta(0) \simeq 1.3$ meV. This yields a gap ratio $(2\Delta/kT_c)$ of 3.3; i.e., these materials appear very BCS-like. Interestingly enough the tunneling data from these and the other 7 successful junctions helped us to identify certain inhomogeneity problems in the manufacture of the commercial ribbon substrates, [2,5] which later enabled us to improve our arc cast $Nb_3(AlGe)$ samples; and, of course, indicated clearly that our ribbon and film substrates were still surface limited.

Further work on improving the substrate surfaces to make them more representative of the bulk resulted in even poorer tunnel barriers, especially the oxide types. Having established, however, at least guidelines for the fabrication parameters of A15 tunnel junctions and realizing that the ribbon substrates, in particular, would always be surface limited because of the conflicting needs of commercial tapes[6] and tunnel substrate

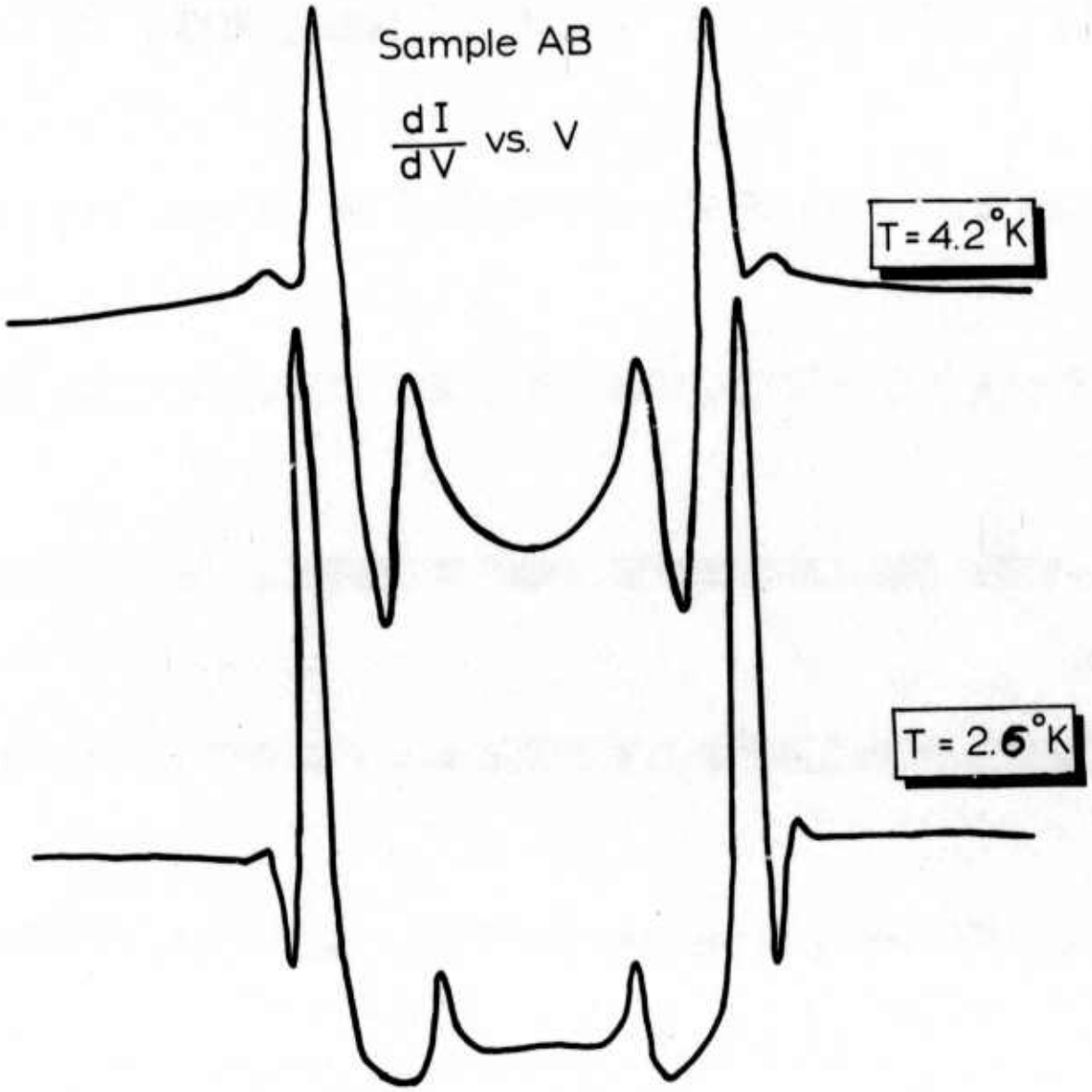

FIGURE 1. CONDUCTANCE CHARACTERISTICS OF RIBBON SUBSTRATE, THERMAL OXIDE BARRIER $Nb_3(AlGe)$ $-Pb_{.7}Bi_{.3}$. JUNCTION RESISTANCE AT 4.2 K WAS 270 Ω.

material, the emphasis of this research was placed on obtaining good bulk substrate junctions.

(ii) Current Research

At the very beginning of the research effort on A15 materials, we attempted to make V_3Au tunnel junctions using arc melted V-Au buttons.[3] Although the buttons were, themselves, homogeneous and better than 90% A15, the problems of deformed surface layers, exterior surfaces not characteristic of the bulk, enormous surface roughness due to their brittle nature, and the inability of the V-alloy systems to oxidize even primitively caused us to focus our attention on preparing bulk substrates using the Nb-based A15 alloys. The combined problems of attempting to perfect the A15 surfaces (with respect to both A15 composition and exposing smooth interior planes for the tunnel barrier) at the same time as the methods for fabricating artificial barriers on A15 substrates were being developed would result in too many possible causes for tunnel junction failure. On the other hand, besides the fact that the highest known T_c A15 compounds are Nb-based [Nb_3Ge, Nb_3Ga, $Nb_3(AlGe)$, Nb_3Al, and Nb_3Sn], it is well known that Nb and its alloys oxidize well. Thus, by switching to Nb-based arc melted A15's we were able to concentrate on the problem of perfecting substrate surfaces, and in a parallel effort worry about developing the art of artificial barrier fabrication (section III of this report).
In addition, other research (ONR and AROD supported) in this laboratory was, and is, centered on understanding the superconductivity of Nb itself,

in the single crystal, polycrystalline, and deformed or cold worked states. The changes which occur in the Nb tunnel junction data as a function of surface deformation should certainly be helpful in determining to what extent our A15 data represents disturbed surface layer tunneling as opposed to true bulk tunneling

Three different bulk substrate materials have been investigated: $Nb_3(AlGe)$ and Nb_3Al which are fabricated using conventional arc melting techniques[9,10] and Nb_3Sn prepared by diffusion of Sn atoms into a Nb substrate.[4] The $Nb_3(AlGe)$ and Nb_3Al samples are fabricated by arc melting stiochiometric powders of the appropriate starting materials (to which an extra 2% by weight of Al has been added) after they have been compacted in a steel die at 36,000 psi. The pressed powders are then melted and mixed such that the sample is turned at least six times while in the melter until the weight loss of the starting preparation corresponds to the desired composition of the final ingot (typically 4 grams in weight). Because of the preferential Al evaporation at these temperatures, it is assumed that the total weight loss is due to Al depletion. We have found that the more mixing and melting that can be achieved with decreasing Al evaporation, the more perfect the samples. The ingots are then subject to a homogenization anneal for 2 hours at 1840 $\pm$ 30C; and the buttons are then quenched to room temperature. The faster this quenching, the less second phase (σ-phase) material present in the final samples. For the $Nb_3(AlGe)$ samples a second low temperature anneal at 725-750 C (10^{-5} torr) increased the mid-point T_c from 17.5-18.5 to a maximum of 18.8 K; for Nb_3Al, to approximately 18 K.

After the anneal, the sample is ground down and cleaved under plane strain conditions to obtain clean, minimally deformed interior surfaces on which to fabricate a tunnel junction.* Finally, the resulting buttons are etched with 10:5:3 (HNO_3, HF, lactic acid) solution for 1/2 minute or anodized in ammonia to determine what phases are present.

Polishing, controlled etching, and electropolishing showed a small amount of second phase (5-10%) in all arc cast samples via the preferential etching and pitting of their surfaces. The etch pit patterns are reminiscent of dislocation site arrays often seen in other transition metal alloys.** In Fig. 2 are shown two typical photomicrographs of the $Nb_3(AlGe)$ samples used in this study. The top picture corresponds to some of our earlier samples which had high porosity and a certain amount of non-A15 phase material; over time (Fig. 2b) we have reduced the porosity but not the 5-10% second phase in these samples (this is probably non-equilibrium Nb or Nb_2Al). Although not shown, the early samples also had wide, clear A15 regions toward the edges of the buttons. We have, therefore, managed to better homogenize our samples by making more uniform

---

*In this procedure the starting ingot is ground to have parallel surfaces. The grinding starts with 600 grit SiC paper through 30μ, 3μ, 1μ, ¼μ diamond pastes, down to 0.6 and 0.06 alumina. (Total time is about 30 minutes.) The surface is then cleaned and rinsed in acetone and the sample cooled to 77K. After placing in a vise, the ingot is struck with a "chisel" perpendicular to the flat surfaces. The surfaces thus exposed are, we hope, more representative of the bulk.

**The question remains, is there a complicated dislocation substructure inherent in the brittle A15 material or are we inducing such a condition by our fracture technique?

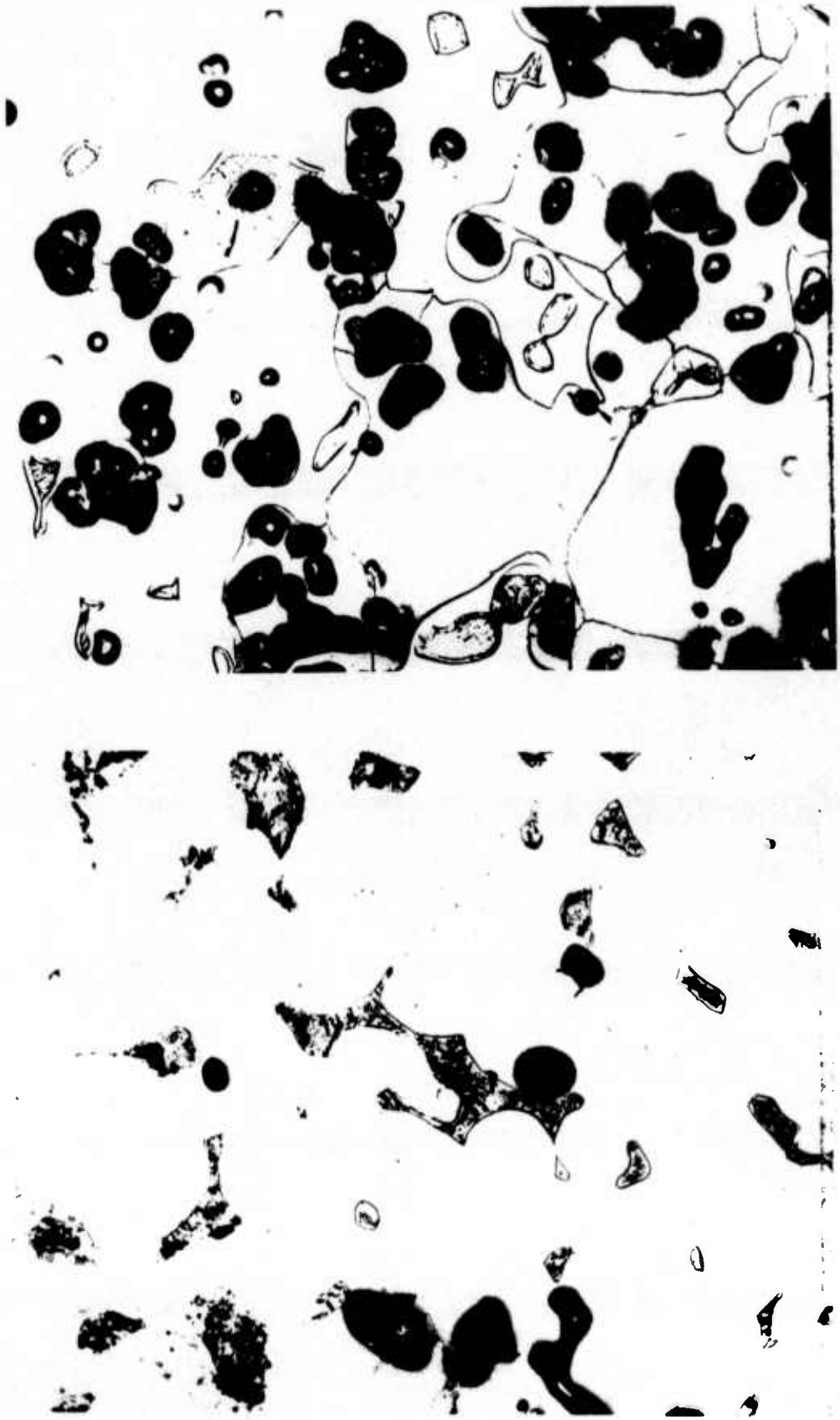

FIGURE 2. PHOTOMICROGRAPHS OF $Nb_3(AlGe)$ ARC CAST SAMPLES (X500) SHOWING POROSITY (BLACK) AND LOW TEMPERATURE SEGREGATES.

A. TOP: TYPICAL BUTTON SURFACE OF EARL WORK.

B. BOTTOM: TYPICAL SURFACES OF MORE RECENT SAMPLES.

the Al depletion. This is also reinforced by the fact that there is less segregation of the phases in the later samples.

Figure 3 is a photomicrograph of the equivalent Nb_3Al samples. (It is only recently that we have fabricated any usable Nb_3Al substrates.) These buttons are 95% A15 phase with the sigma phase segregated in small volumes in the sample. This indicates that the coring, occuring during arc melting, has not been completely eliminated upon high temperature annealing. It should also be noted that these samples show a much higher porosity than the $Nb_3(AlGe)$ probably because the Ge suppresses the Al activity in the latter compound. However, the Ge samples tend to have much larger cavities ($\sim 1\mu$) than the Al and they are not so uniformly distributed across the sample surface, which is also true of the second phase component. It is, perhaps, these facts which explain why the tunneling into Nb_3Al is so superior to that in the $Nb_3(AlGe)$.

Several methods have been used to fabricate junction barriers on the bulk substrates, the particular one in any case depending on the nature of the surfaces: surface etching followed by glow discharge oxidation, controlled-chemical etching of barriers, oxypolishing (or anodic stripping) of the sample substrate; and finally, artificial barriers which includes flash evaporation of thin Al layers followed by complete layer oxidation, or use of semiconductor layers. All of these methods have resulted in identifiable superconducting tunnel characteristics. In combination, moreover, they have been even more successful. In the following we choose only to discuss the particular method which seemed best for a given substrate. So, for example, Al_2O_3 layers on $Nb_3(AlGe)$ resulted

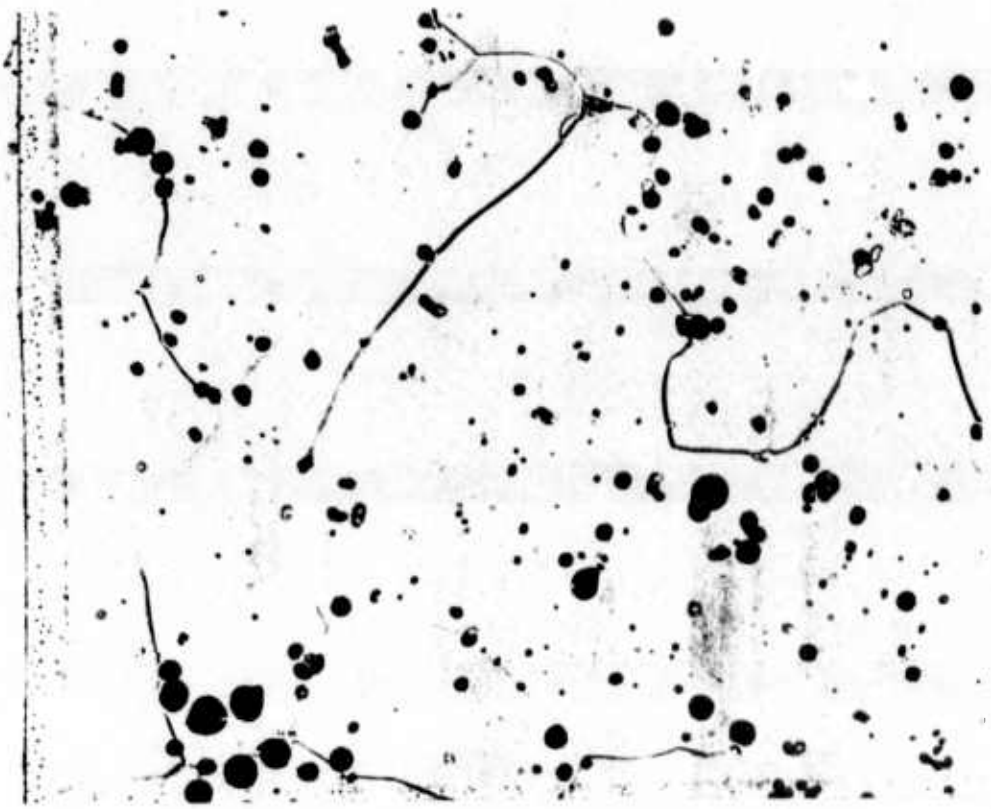

FIGURE 3.
PHOTOMICROGRAPH OF ARC MELTED Nb_3Al (X500) SHOWING POROSITY (BLACK) AND SMALL AMOUNTS OF SEGREGATED σ PHASE.

in 0.3Ω junctions (but whose tunnel characteristics were no better than junctions with oxide barriers) will not be reported. Junctions were then completed by depositing a $10^{-6}\mu$ Pb film* on the barrier and attaching Au leads to the sandwich configuration with Ag paint. The tunneling area was typically 1/4 X 4 mm. As a final step the junction was coated with formvar to preserve it.

To date the most successful** barriers on samples obtained by sintering elemental powders have been formed by mechanically and/or chemically polishing*** the button surfaces before subjecting them to a glow discharge oxidation in 50μ of oxygen at ≈750 V for 15-30 minutes. Junctions made on "exterior" fractured surfaces were unstable with respect to temperature cycling and time, and often yielded data not inconsistent with a normal layer on the A15 surface despite the fact that the bulk T_c was 18 K or higher. Some few junctions had characteristics in which distinct structure belonging to Pb could be identified. Junctions made on "internal" A15 surfaces were far more stable and in a few cases exhibited ordinary tunneling structures: sum and difference peaks, multiparticle peaks, etc. We are encouraged by these results since, as previously discussed, these surfaces are characterized by etch pits,

---

*Earlier we used Pb-Bi stripes which can be difficult to fabricate.[11] We subsequently found that the counter electrode deposition is even more important than we thought[12] so we converted to Pb thin films which are both stable and easily controlled.

**That is, giving the largest non-shorted, non-linear characteristic junction yields.

***In a 1:4:5 (HF, HNO_3, H_2SO_4) electropolishing solution.

bubbles, and second phase contamination. This lack of uniformity and smoothness precludes, we feel, the fabrication of good tunnel junctions because the thickness of the barrier layer is then, in turn, non-uniform which will give rise to shorts and microbridges, both phenomena often observed in our samples.

A tunnel derivative characteristic of our best $Nb_3(AlGe)$ junctions is given in Fig. 4; it clearly represents S-I-S' tunneling although its shape is far from ideal. Other experiments on deformed Nb, in this laboratory* are the basis of our speculations on the positions of the A15 multiparticle peaks and the gap edge structure. Figure 5 shows the first derivative of an annealed polycrystalline Nb foil, which has, of course, ideal shape.[13] Figure 6 shows the change in tunneling characteristic when the foil is swaged and rolled to give a true strain of 9.3.** Both of the first derivaties shown in Fig. 6 seem to be typical of these highly deformed surfaces.[13] The comparison between Figs. 4 and 6 is obvious and leads us to believe that we still are tunneling into a highly deformed A15 surface. Other characteristics obtained on the Nb foils which map the change in sample conductance as a function of deformation from zero strain to 9.3 will be used to check our surface conditions as we continue to improve our $Nb_3(AlGe)$ samples.

For purposes of comparison we have also included a tunneling characteristic for Nb_3Al in Fig. 7. It has an ideal conductance shape with both gap

---

*AROD-supported.

**We thank Mr. Nathan Cheung for providing us with this data for our report.[13]

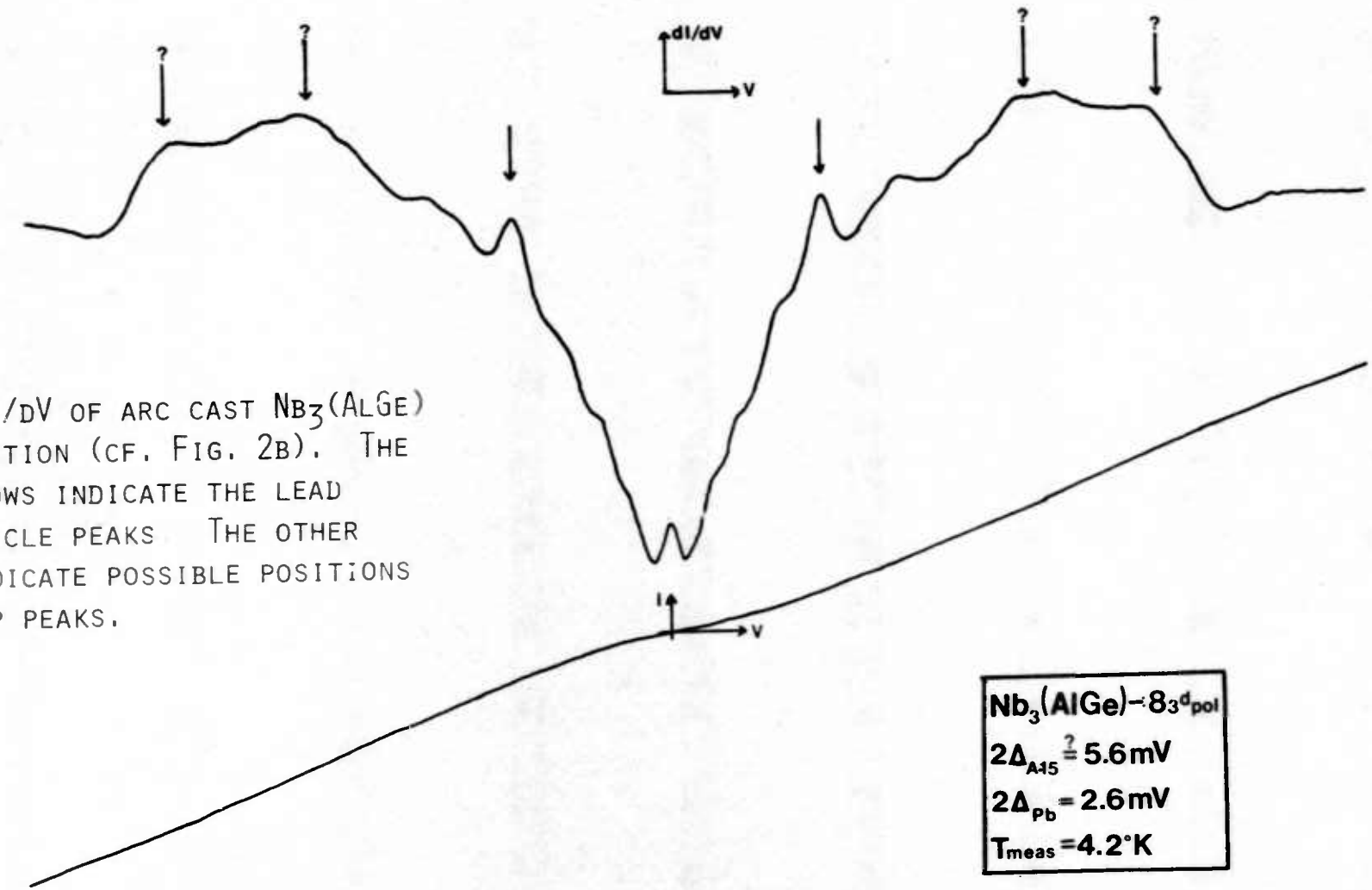

FIGURE 4.
I-V AND dI/dV OF ARC CAST $Nb_3(AlGe)$ OXIDE JUNCTION (CF. FIG. 2B). THE PLAIN ARROWS INDICATE THE LEAD MULTIPARTICLE PEAKS. THE OTHER ARROWS INDICATE POSSIBLE POSITIONS OF SUM GAP PEAKS.

FIGURE 5
THE NEARLY IDEAL FIRST DERIVATIVE CURVE FOR AN ANNEALED POLYCRYSTALLINE NB-IN SAMPLE. THE INSET CURVE IS A MAGNIFICATION OF THE LOW AMPLITUDE IMMEDIATELY BELOW IT. ARROWS INDICATE THE MULTIPARTICLE PEAKS FOR BOTH NB AND IN.

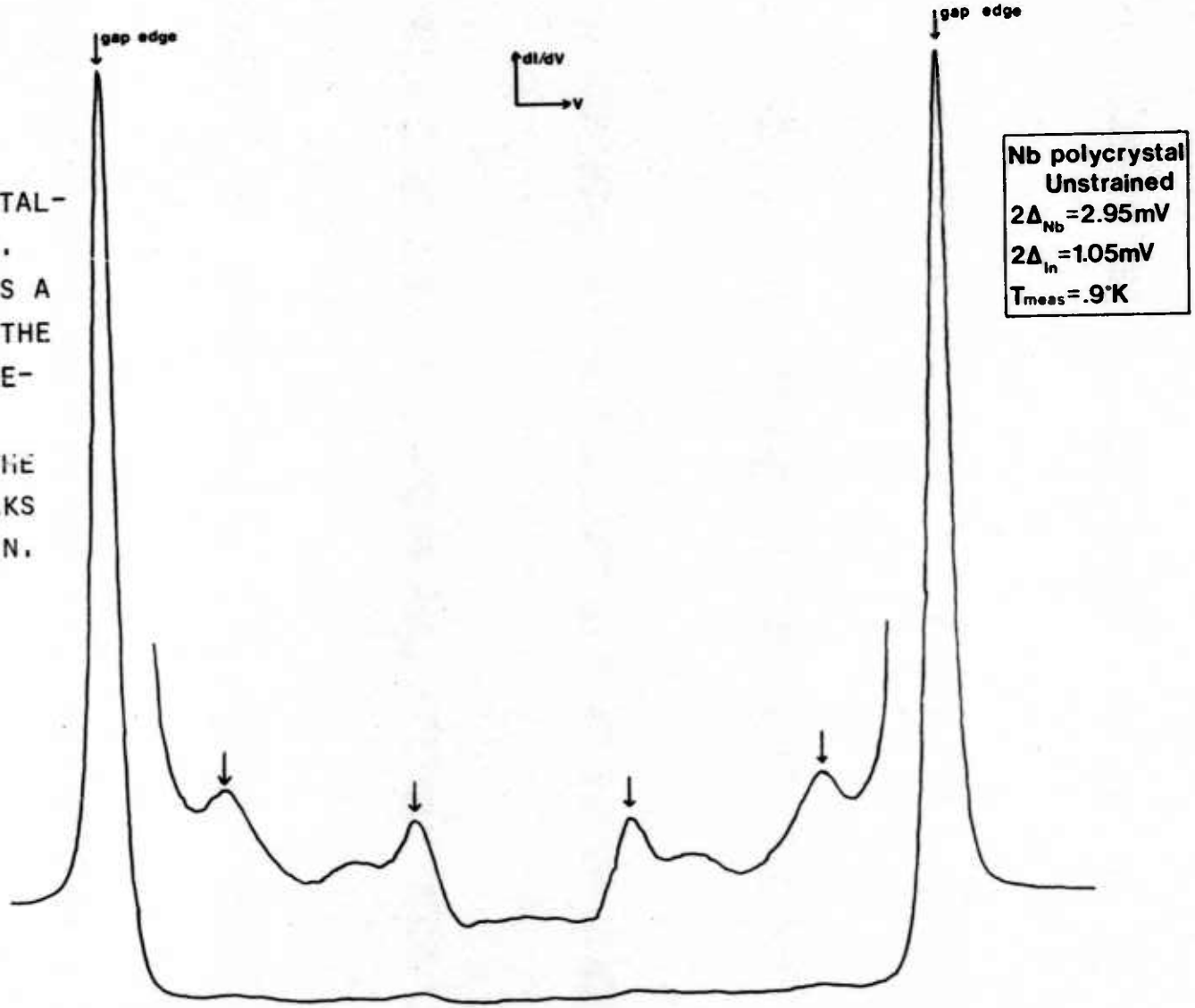

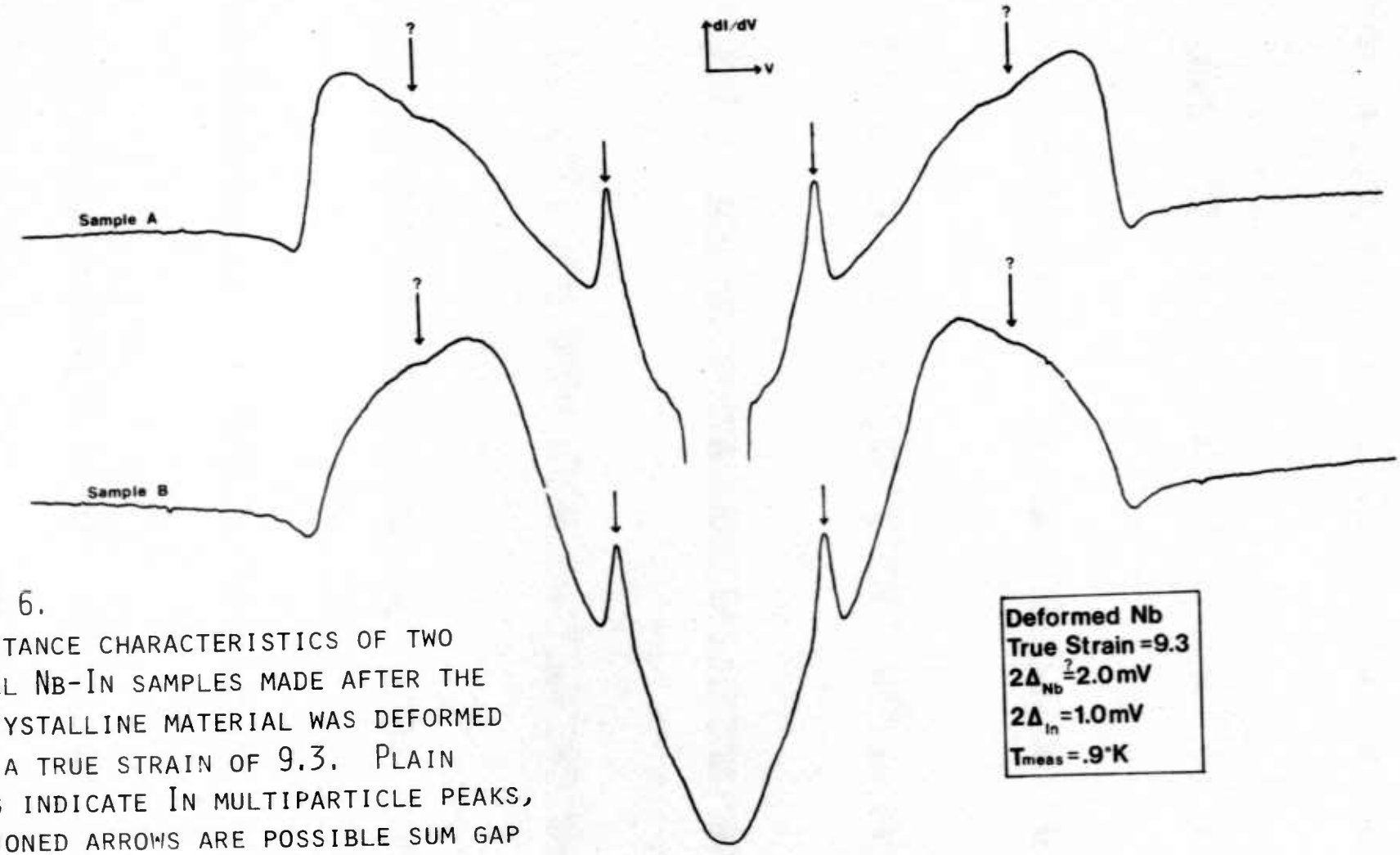

FIGURE 6.
CONDUCTANCE CHARACTERISTICS OF TWO TYPICAL NB-IN SAMPLES MADE AFTER THE POLYCRYSTALLINE MATERIAL WAS DEFORMED UNDER A TRUE STRAIN OF 9.3. PLAIN ARROWS INDICATE IN MULTIPARTICLE PEAKS, QUESTIONED ARROWS ARE POSSIBLE SUM GAP PEAKS.

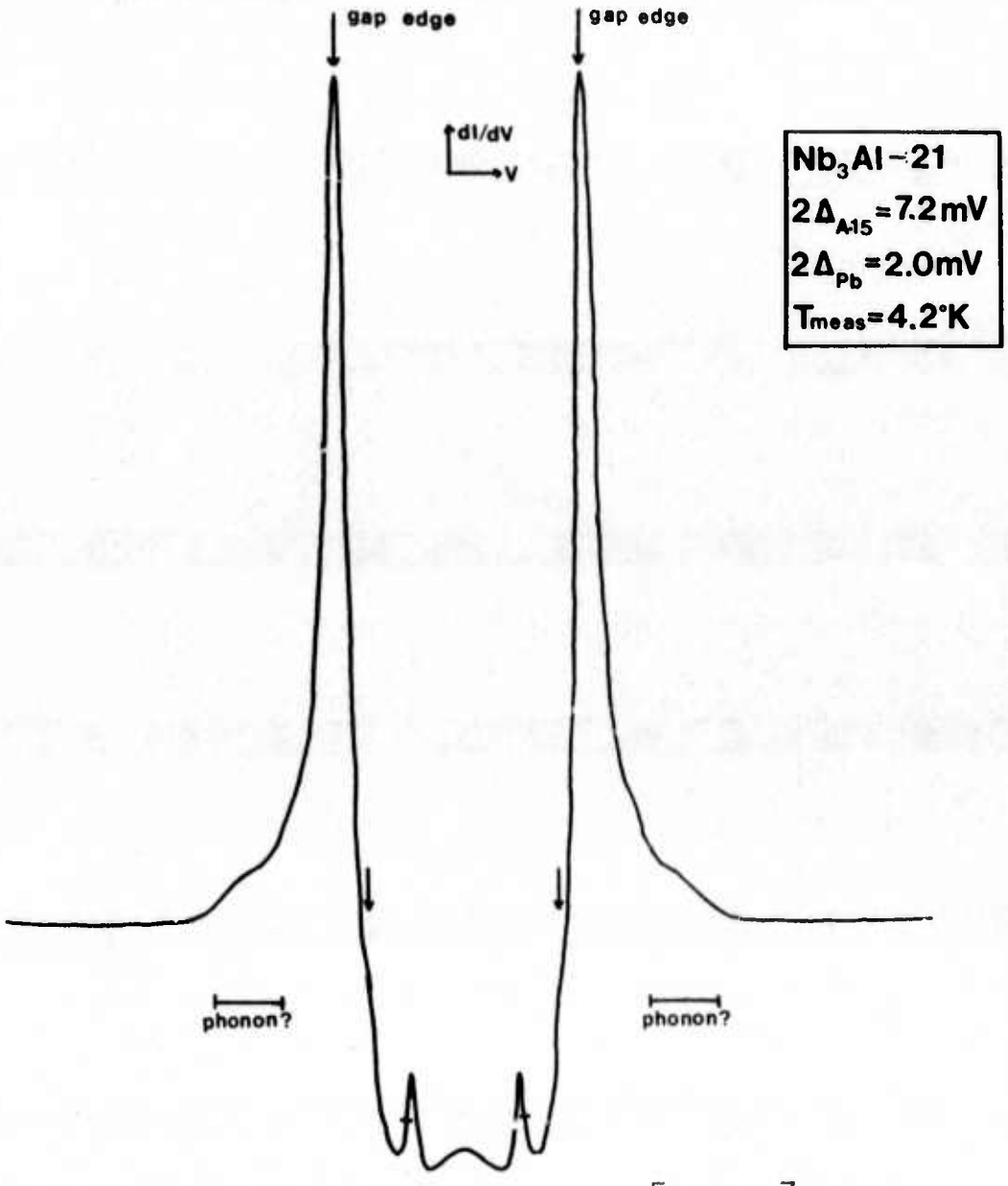

FIGURE 7.
FIRST DERIVATIVE CURVE OF ARC MELTED Nb_3Al JUNCTION (SEE FIG. 3) WITH PB COUNTERELECTRODE. ARROWS INDICATE POSSIBLE A15 MULTIPARTICLE PEAKS; THE BAR DENOTES THE CUSP ON THE DIFFERENCE PEAK.

edge and difference peak. As can be seen, however, the low value of the A15 gap indicates that we are observing BCS-like behavior (i.e., $2\Delta/kT_c \sim 3.3$). Our previous experience with thin films and ribbons indicates that this tunneling also represents a surface limited condition so that, in fact, the effective T_c of the A15 in the tunnel junction is less than the bulk $T_c \sim 16$-17K. Experiments to determine this are in progress. On the other hand, the absence of the Pb multiparticle peak indicates that a good uniform tunnel barrier has been formed. Whether the latter is due to the lack of substrate surface perfection remains to be seen.

Recently a new technique[4] for preparing high quality, high T_c Nb_3Sn diffusion layers has been perfected by Siemens Laboratory for use in high Q superconducting microwave cavities. They report it results in very smooth homogeneous bulk-like A15 material, the smoothness depending on the surface roughness of the underlying Nb sample into which Sn atoms are diffused. We have adapted their procedures to obtain our Nb_3Sn substrates. We have not had time, however, to optimize our fabrication procedures. In order to obtain a clean smooth Nb starting surface, 1/8" Nb single crystal rods were grown in our ultra-high vacuum electron beam floating zone apparatus. This rod is then sealed in a quartz ampule with a saturated Sn atmosphere at 1000C for 20 hours. During this time Sn atoms diffuse into the niobium and then react to produce a Nb_3Sn layer several microns thick (up to $\gtrsim 4\mu$). The reacted cylinders are then removed from the ampule and oxypolished up to 5 times (to 100V each time) to remove the outer non-stoichiometric surface layers of the

sample. After polishing they are rinsed in water and methanol and dried in an evacuated desiccator. The T_c of such samples is 16.5K; optimizing the fabrication parameters in the growth technique should result in $T_c \gtrsim 18K$.

If the counter-electrode is deposited on these samples immediately after oxypolishing the barriers obtained are unstable and noisy, if not shorted. By backfilling the desiccator with an atmosphere of oxygen and allowing the samples to oxidize for 20-30 hours, good stable junctions have been obtained. To date we have tested 15 junctions: 8 were shorted, 2 had strange structure as seen in the $Nb_3(AlGe)$ junctions, and 5 resulted in the so-called Werthamer junctions.[14] Although the latter are thought to be symptomatic of very thin non-uniform barriers layers, they are interpretable and reproducible not only from junction to junction but when the same junction is tested over a period of days. Junction resistances range from 10 to 500 Ω. Unfortunately, the junctions still have large background and leakage currents which obscure the structure at the sum-gap bias so that the sum peak cannot be unequivocally identified, and therefore, there is no conclusive evidence that our interpretation of the observed tunneling structure is correct.

The first derivative curve of a typical junction is shown in Fig. 8. The Pb double particle peak (dpp) appears at ∿1.4 mV with associated multiparticle peak structure (mpp) at bias values of Δ_{Pb}/n where n = 1,2,3,... Similarly, there is a peak at ∿3.6mV and corresponding structure at 3.6/n. We have tentatively interpreted these features as the dpp and mpp of the Nb_3Sn. This can only be verified if we can improve our junctions so that

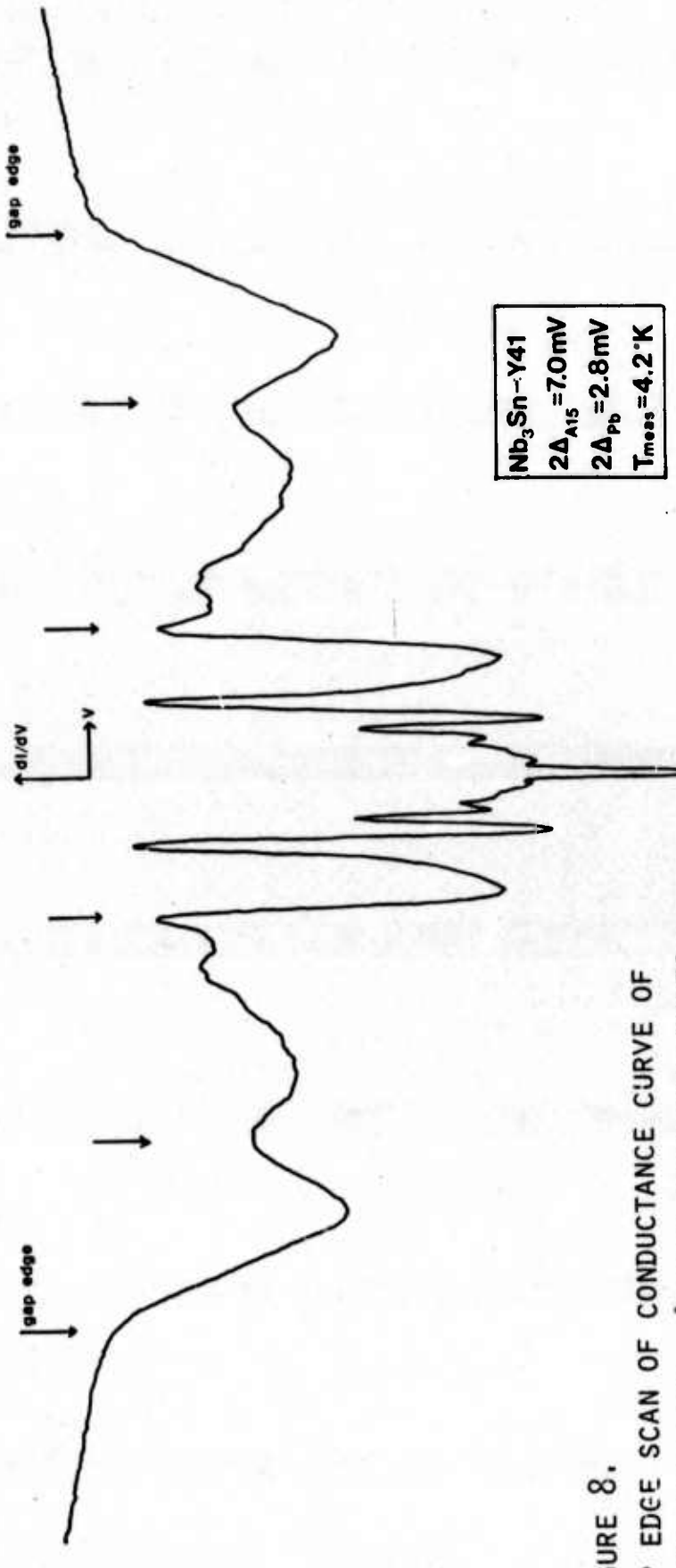

FIGURE 8.
GAP EDGE SCAN OF CONDUCTANCE CURVE OF Nb_3Sn JUNCTION. ARROWS INDICATE MULTI-PARTICLE PEAKS OF THE COUNTERELECTRODES. ARROWS DENOTED AS "GAP EDGE" INDICATE THE CALCULATED POSITIONS OF THE SUPPRESSED SUM GAP PEAKS.

the gap edge is visible on the derivative. With reference to the deformed niobium work and previous investigations in this laboratory on single crystal Nb-In junctions, the change in slope indicated by the "gap-edge arrow" in the figure should locate the sum gap peak. If this is correct, then $2\Delta/kT_c$ for these samples is 5.2 indicating extremely strong coupled superconductivity in these materials. Clearly, our next step will be to try to eliminate the background current so that the sum-peak can be observed, thus putting our interpretation on a firm basis.

In Fig. (9) a conductance scan of another of the Nb_3Sn junctions shows the characteristic phonon structure that should be present in superconducting Pb junctions. The first two peaks (measuring from the zero bias) have the proper position for Pb, the last structure may be one peak of the Nb_3Sn phonon spectrum. The relative ease with which these reacted layer substrates produce good junctions is extremely encouraging. We are attempting, at the present time, to improve the substrate surfaces in combination with exploring various other means to fabricate the oxide barriers on these surfaces.

DATA ANALYSIS*

Electron tunneling has come to be recognized as one of the most important techniques for studying the properties of metals in both the superconducting and normal metal states. In a tunnel junction if one (or both) of the metals is in the superconducting state at least four important properties

---

*This work was completed in conjunction with other ONR-supported research,

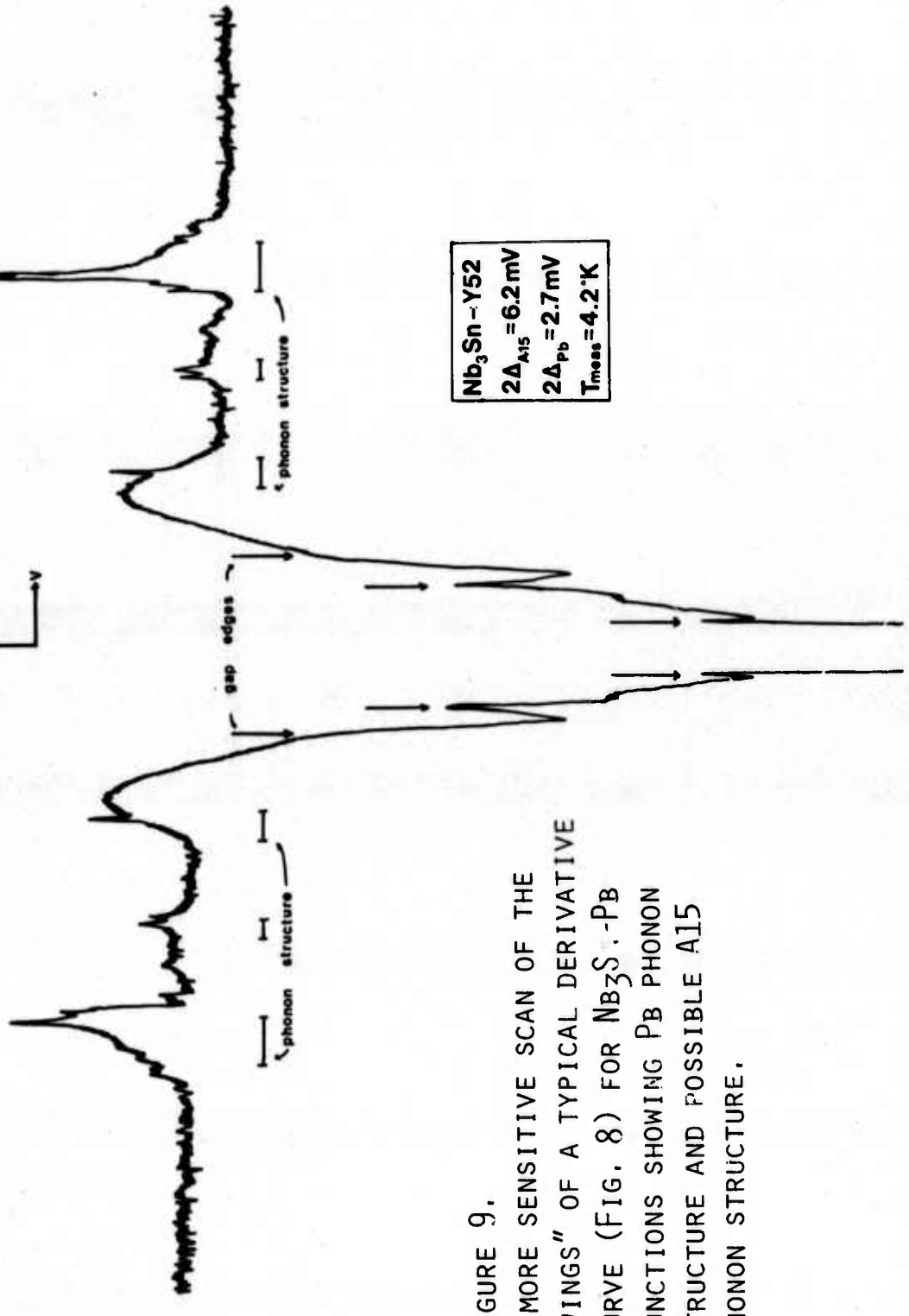

FIGURE 9.
A MORE SENSITIVE SCAN OF THE "WINGS" OF A TYPICAL DERIVATIVE CURVE (FIG. 8) FOR Nb_3Sn-Pb JUNCTIONS SHOWING Pb PHONON STRUCTURE AND POSSIBLE A15 PHONON STRUCTURE.

of the metal(s) can be determined from the first derivative characteristic*: the elctronic density of superconducting states N(E), the electron coupled phonon spectrum $\alpha^2F(\omega)$ [which is proportional to the phonon density of states $F(\omega)$], the electron-phonon coupling constant λ, and the BCS superconducting gap value Δ_o. Until recently, such experiments have been limited to using a normal metal (or a BCS superconductor) as the counterelectrode in tunnel junctions because of numerical difficulties in interpreting data obtained from junctions having mixed strong coupling superconductors as counterelectrodes. However, it is known that the quality of the tunnel junction depends on the counterelectrode materials[12] and, in particular, the best transition metal junctions are obtained using other strong coupling superconductors as counterelectrodes. Although the initial research in developing a method of data analysis for such junctions, reported below, refers specifically to Nb, the potential applications in tunneling experiments with A15's are obvious.

The difficulty in unraveling the tunneling data can be understood from the following two considerations. First, the experimentally measured current is**

$$I(V) \sim \int_{-\infty}^{\infty} N_1(E)\, N_2(E - eV)\, dE$$

---

*The conductance curve, dI/dV - V.

**The concepts involved in superconductive tunneling and a detailed explanation of data deconvolution are given in both entries of Ref. (15) and also in Refs. (16) and (17).

where V is the bias voltage and $N_i(E)$ is the density of states of a given side of the junction as a function of the energy E. This means that the first derivative, which contains the most accurate phonon information is:

$$\frac{dI}{dV} \sim \frac{d}{dV} \int_{\Delta_1}^{V-\Delta_2} N_1(E)\, N_2(E - eV)\, dE$$

where Δ_i is the energy gap value of a given side of the junction. The first job of the data analysis is thus to find the density of states, say N_2, given N_1 of the known counterelectrode and the experimental $\frac{dI}{dV}$ data. (The gap values Δ_1 and Δ_2 can be read directly off the derivative curve.[12]) The second task of the analysis is to relate this electronic density of states to the phonon properties of the material.[15,16,17] This is done by solving the Eliashberg equations for the superconducting state.* However, these are integral equations expressing the complex gap function $\Delta(E)$ in terms of a kernel which is itself dependent on the gap function.

There are, clearly, a myriad of solutions to these equations and the particular solution for a given material can be determined only when appropriate boundary conditions are imposed on the solutions. In

---

*These are given on the next page: μ^* is the dimensionless Coulomb pseudo-potential and the electron-phonon coupling constant

$$\lambda = 2\int_0^{\omega_o} \left[\frac{\alpha^2 F(Eq)}{Eq}\right] dEq \quad .$$

Equations To Be Programmed

$$\phi(E) = \int_{\Delta_o}^{\omega_c} dE' \left[\mathrm{Re} \frac{\Delta(E')}{\sqrt{E'^2 - [\Delta(E') \cdot \Delta(E')]}} \right] \{ K_+(E',E) - \mu^* \}$$

$$\sum(E) = \left[1 - Z(E) \right] E = \int_{\Delta_o}^{\infty} dE' \left[\mathrm{Re} \frac{E'}{\sqrt{E'^2 - [\Delta(E') \cdot \Delta(E')]}} \right] \{ K_-(E',E) \}$$

where

$$K_\pm(E,E') = \sum_{\text{pol.}} \int_0^{\infty} dE_q [\alpha^2 F(E_q)]_{\text{pol.}} \left\{ \frac{1}{E' + E_q - i\delta + E} \pm \frac{1}{E' + E_q - i\delta - E} \right\}$$

$$Z(E) = 1 - \frac{\Sigma}{E} = 1 - \frac{1}{E} \int_{\Delta_o}^{\infty} dE' N(E') K_-(E',E)$$

$$N(E) = \mathrm{Re} \frac{|E|}{\sqrt{E^2 - [\Delta(E) \cdot \Delta(E)]}}$$

$$\Delta(E) = \phi(E) / Z(E) = \Delta_R(E) + i \Delta_I(E)$$

such that $\Delta(E) \cdot \Delta(E)$ is a complex number,

$\Delta(E) \cdot \Delta^*(E) = \Delta^2(E) = \Delta_R^2 + \Delta_I^2$,

$\Delta_R(E = \Delta_o) = \Delta_o$ (BCS-value)

$\Delta_I(E = \Delta_o) = 0$.

tunneling experiments it is possible to determine exactly the density of states of the material and the value of the gap edge $\Delta(\Delta_o) = \Delta_o$ directly from the experimental data. The final analysis stage associated with these experiments amounts to using these two constraints to determine the complex functions described by the Eliashberg equations (on a digital computer) and to obtain the electron-coupled phonon spectrum, α^2F, upon which these functions depend.

In essence the analysis can be divided into 3 separate parts or "STAGES". The first, Stage I, is a raw data processing step. It takes the lock-in amplifier output along with the DC bias as input data and determines the smoothed normalized conductance of the tunnel junction at a constant bias interval. STAGE II is concerned with the deconvolution of this conductance data to reflect only the density of states of the junction electrode being investigated; i.e., the normalized conductance and the density of states of the "known counterelectrode" are used to produce the electronic density of states of the unknown electrode as output. This output is used only for reference purposes in STAGE III. This final stage of the analysis consists of numerically solving the Eliashberg equation for $\Delta(E)$, $\alpha^2F(\omega)$, λ, and μ^*. This is done by assuming various functional forms for $\alpha^2F(\omega)$ and $\Delta(E)$ and interactively solving all of the equations to obtain self-consistency. After self-consistency for a given set of "guesses" Δ and α^2F has been obtained, a density of states [N(E)] is calculated from this solution. This calculated function is then compared

to the output of STAGE II, the so-called "experimental" density of states. The set of "guesses" for $\Delta(E)$ and $\alpha^2F(\omega)$ which gives the "experimental" N(E) is the true solution to the Eliashberg equations for the particular metal in question.*

The initial programming for data analysis that we received[16] was capable of extracting electron-coupled phonon spectra from S-I-N junctions and, with some loss in precision, from strong coupled superconductor-BCS superconductor junctions. Major changes have been made in two of the 3 program stages. (1) The first modification is a program introduction comprised of all the software necessary to convert the output of the conventional tunneling electronics into absolute data characteristics. (2) The second stage has been extensively revised to allow the analysis of S-I-S' junctions with strong coupled superconductors on both sides of the barrier. The numerical accuracy of this stage has also been improved by more than an order of magnitude. The constraint of having only one unknown material in the junction remains, however.

Only minor modifications were necessary in STAGE III. After revising this program with improved numerical routines, the total double interactive procedures and convergence checks which were disabled susequent to the initial investigation of the Pb phonon spectrum were reimplemented. STAGE III is, thus, capable of deconvoluting phonon spectra to a self-consistency of better than one part in 10^4. Other, minor computer

---

*The sequence of guesses is NOT random but determined by a linear feedback routine which is based on how the calculated and experimental N(E)'s differ.[15,16,17]

routines necessary for preparing input to the main program (especially STAGE II) were also written and tested. The net result of these modifications is, we feel, an inversion routine which has greater accuracy and flexibility than the original programming, is more specific in the raw data handling techniques, and finally has a far wider range of applications than previously possible.

Single crystal Nb data has been used to determine the viability of the double deconvolution software.[17] First, we extracted the phonon spectra from Al-In and Al-Pb film junctions assuming Al is a BCS counterelectrode. The In results, determined from tunneling data taken at 1 K, compare extraordinarily well with spectra determined at .3 K. The Pb spectrum (also at 1 K) was far better than previously determined spectra from Al-Pb junctions, but not as good as those determined from Pb-Pb tunneling data. Three types of Nb junctions were analyzed: Nb-Au (Au is normal), Nb-In (In is an intermediate coupled material), and Nb-Pb (Pb is a strong coupled element). The spectra from all three types (11 junctions total) agree in all significant respects. A typical characteristic is shown in Fig. 10. Not only did the same shape result from all the spectra investigated, but this shape agrees with the phonon spectrum determined from neutron scattering.[18] This spectrum is shown in Fig. 11.

---

*The characteristic of these calculated spectra which differs most from the neutron scattering results involves the height of the longitudinal peak. As shown in the neutron scattering phonon spectrum, the longitudinal peak is always $\gtrsim$ twice as high as the transverse peak. The best tunneling phonon spectrum ever obtained (Pb) has only equal height peaks,[16,17] This is thought to be due to the energy dependence of the electron coupling function $\alpha^2(\omega)$. Other conjectures are discussed in Ref. (17), pp. 127,143.

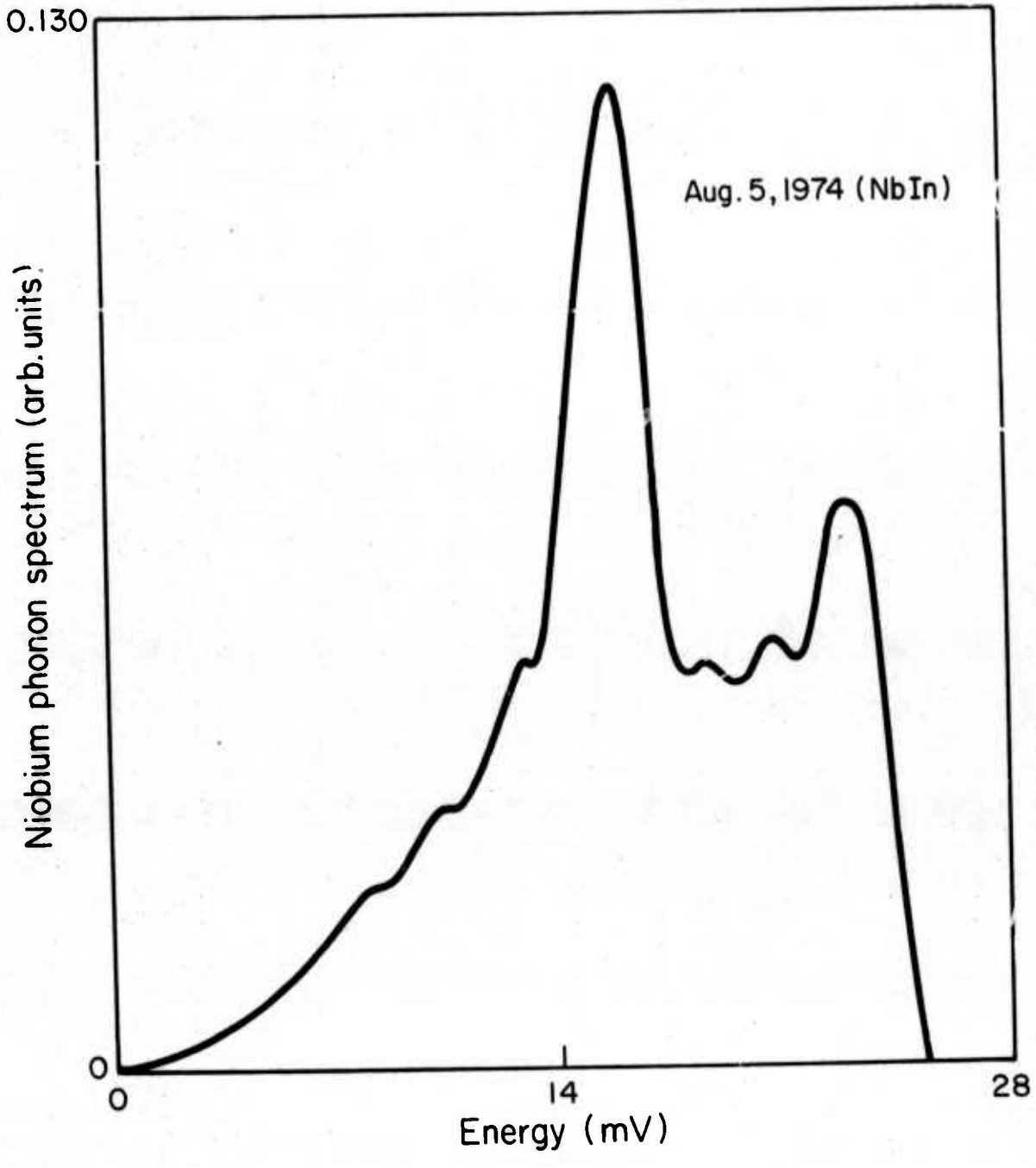

FIGURE 10. NB PHONON SPECTRUM DECONVOLUTED FROM A SINGLE CRYSTAL NB-IN JUNCTION: RESISTIVITY RATIO OF NB = 483; $\mu^* = -.11$; $\lambda = .4$.

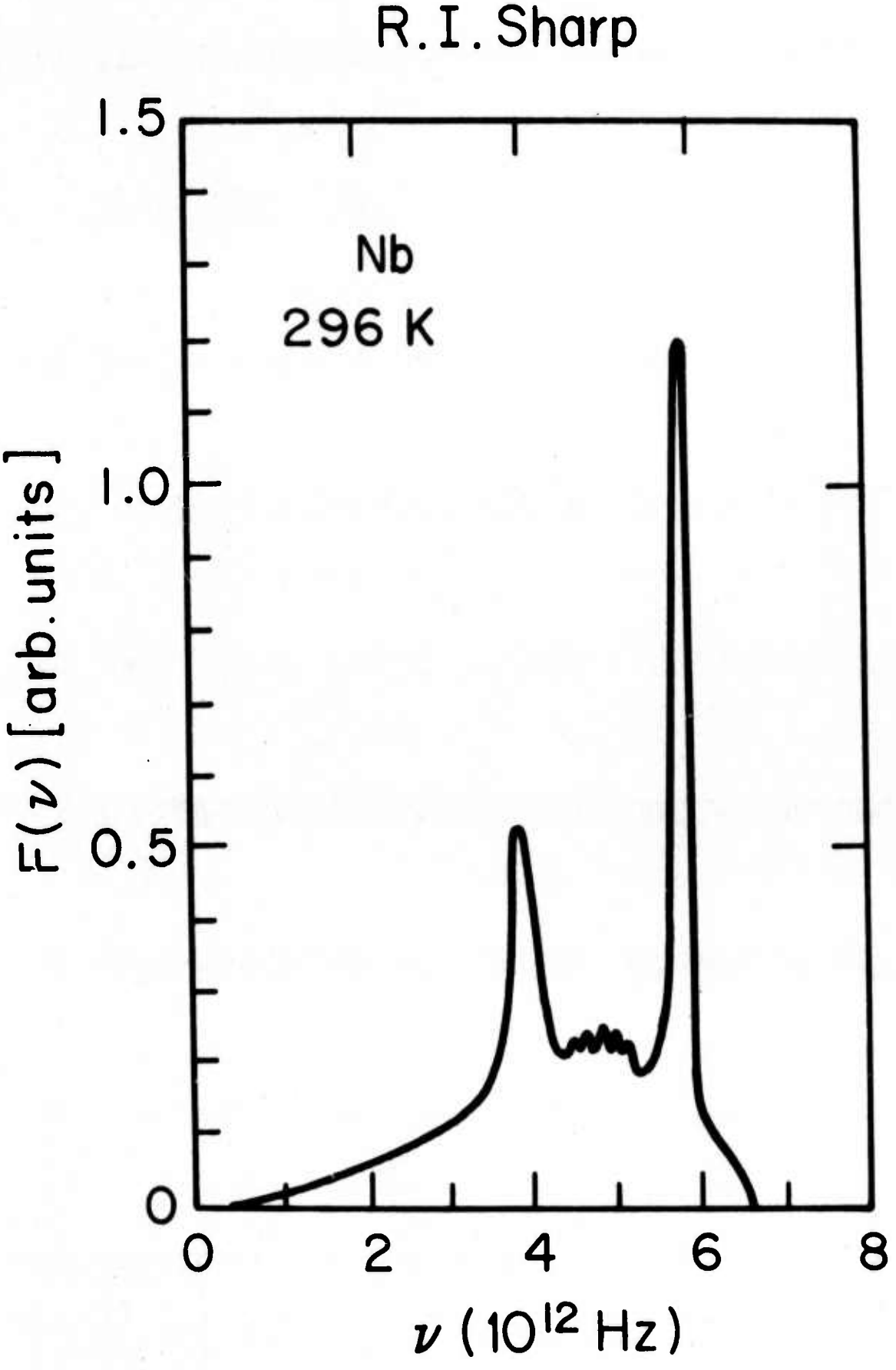

FIGURE 11. NB PHONON SPECTRUM AS CALCULATED FROM INELASTIC NEUTRON SCATTERING: R.I. SHARP, J. PHYS. C(SOL. ST.) 2 (L969) 421 AND 431.

In order to determine whether the deconvolution routines resulted in different α^2F's when the surfaces of the tunneling substrate were known to be dirty, impure, or deformed, we purposefully "contaminated" the single crystal Nb cylinders. In one case, holding all other fabrication parameters constant, the growth rate of the single crystal was doubled. The resulting crystal had visible rings around the crystal cylinder which probably are due to the uneven growth and segregation of the impurities in the melt into impurity bands. The α^2F function generated from this junction is shown in Fig. (12a). The first two peaks can be seen to have grown at the expense of the longitudinal peak at the end of the spectrum. A second Nb junction was made by strongly etching the surface of the single crystal with acid before the oxidation forming the barrier (all other fabrication parameters were held constant). The results obtained from that junction are shown in Fig. (12b). The main change from the junctions representative of the pure single crystal is seen in the splitting of the longitudinal peak and the increased shoulder structure between the peaks. These results do not agree with the neutron work and indicate that the computed α^2F is very sensitive to the conditions of the surface of the Nb single crystal. As a matter of interest it should also be noted that the first derivative scans from gap edge to gap edge were not that different for the three samples described; only their phonon characteristics were distinctly different.

There is, on the other hand, a disturbing discrepancy in the values of λ and μ^* computed from the single crystal Nb data: parameter values from different junctions did not compare well,[17] nor did any set of these values agree with theoretically accepted values. The most alarming

FIGURE 12. THE ELECTRON COUPLED PHONON SPECTRUM OF SINGLE CRYSTAL NB-I-IN JUNCTIONS:

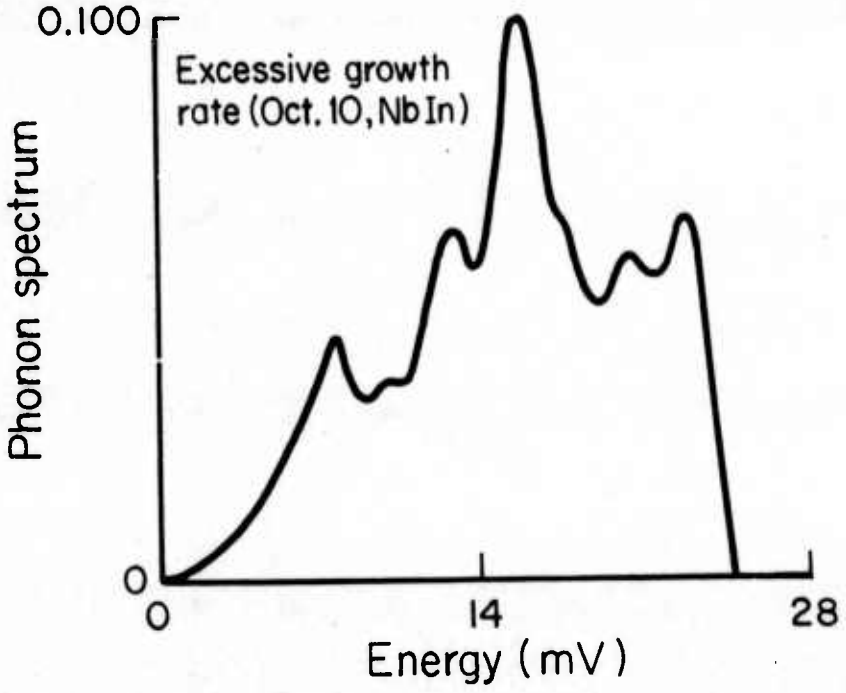

(A) NORMAL CRYSTAL GROWN RATE DOUBLED;

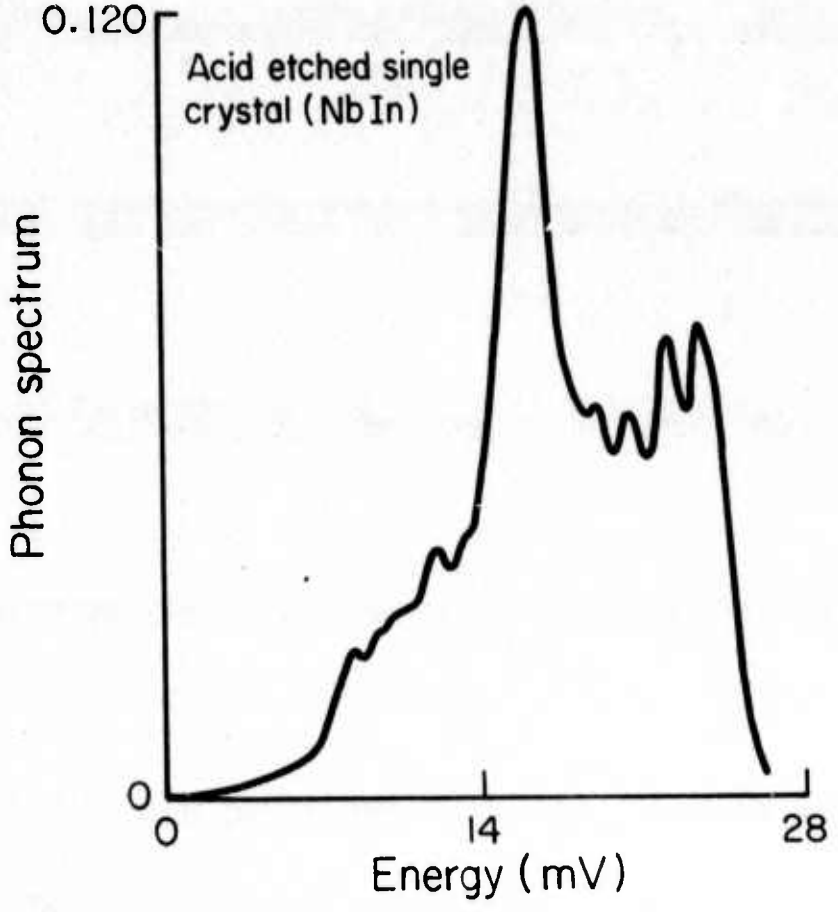

(B) NORMALLY GROWN CRYSTAL SUBJECT TO AN ACID ETCH BEFORE BARRIER FORMATION.

result is that all calculated values of μ^* are negative. In fact, a negative value of μ^* has no physical meaning within the Eliashberg theory of strong coupling superconductors since it represents the effective value of the Coulomb repulsions between the electrons. Such a value could mean, of course, that there exists some other positive electron interactions besides the electron-phonon interaction which has not been taken into account for transition metal compounds. (Or, perhaps, it is also possible that this effect is due to the very complicated Fermi surface and high density of d-electrons in Nb.)

On the other hand, the α^2F spectrum obtained when μ^* is negative carries all the essential features of the neutron scattering data so that this possibility seems unlikely. And, most other studies NOT carried out on simple, isotropic s-p band materials have resulted in anomalously low (and even negative) values of μ^*. It is not, however, obvious what the difficulties are*; they might be experimental in nature, be an artifact of the numerical calculations, or be of a fundamental nature.

A number of "model" phonon spectra, based on both our work and the neutron scattering results, were devised for Nb in order to determine: exactly how the self-consistency routines would handle the convergence toward this spectrum, precisely what values of μ^* and λ would be characteristic of Nb given the ideal phonon shape, and whether the programming would discriminate against generating a negative μ^*. Although there is no preference in the programming for either positive or negative μ^*, the convergence for

---

*A detailed discussion of the possibilities can be found in Ref (17), pp 127-143.

negative values is far slower. Ideal Nb spectra can be generated with positive μ^* but then the values of λ are absurdly high.

As an external (rough!) check on the validity of such spectra, T_c was calculated using the commonly accepted approximations inherent in strong coupled superconductivity (and, thus, our programming):[19]*

$$T_c = \frac{\langle\omega\rangle}{1.2} \exp\left[\frac{-(1.04)\ (1 + \lambda)}{\lambda - \mu^*\ (1 + \frac{\langle\omega\rangle}{\omega_o}\lambda)}\right] .$$

Values of the parameters generated by our actual experimental data produced good agreement with the measured T_c values. The ideal phonon spectrum results were factors of 3/2 and more, higher than measured T_c's. A careful consideration of the basis of this equation, however, has convinced us that for a material with a very broad phonon spectrum, especially with phonon structure below 10 mV, accurate values of T_c can be produced only by a full self-consistent solution of the finite temperature Eliashberg equations.

---

*The first moment of the phonon spectrum $\langle\omega\rangle$, is also generated by STAGE III.

(iii) Direction of Future Work

We plan to continue to improve the quality of our arc melted samples surfaces and to experiment with different methods for producing tough, durable oxides on these substrates. We will also continue to use a variety of other substrate sources such as films and reacted Nb cylinders The object is, of course, to obtain internally consistent, high quality tunneling data which can be used with the deconvolution software to extract the phonon spectra and strong coupling parameters characteristic of bulk A15's.

We have recently obtained the Nb_3Sn single crystal from the RCA Laboratory in New Jersey. When we feel we have optimized our barrier oxidation techniques we will use the data from this crystal in a comparison with our reacted Nb_3Sn cylinders to determine the quality of our surface layers and to determine differences in their phonon spectra.

We have already begun to investigate the possibility of developing a reacted Nb_3Al cylinder by encapsulating a Nb single crystal and Al vapor in a constant volume Nb shell. Since this method is based on the same principles as those involved in reacting Nb with Sn vapor, we believe we can produce bulk-like surfaces of ordered Nb-Al A15 with a surface composition varying between 19 and 28 atomic percent. At present, liquid metal corrosion of the Nb container limits the treatment time possible for reacting the sample, better temperature control in the process is needed, and the geometry must be redesigned so there is a uniform diffusion of Al into the Nb single crystal.

Since it is highly probable that the deconvolution of the A15 materials will be done with 4 K tunneling data, we are presently programming the finite temperature Eliashberg equations of superconductivity. At the same time we are attempting, experimentally, to fabricate and deconvolute superconducting In-Pb junctions to determine the ultimate capabilities of the double deconvolution routines for zero temperature. This is necessary because there is no way of knowing if the phonon spectra of Pb and some particular A15 compound entirely overlap, as do the spectra of Pb and In (whereas that of Pb and Nb, e.g., do not). In addition, we are continuing our study of the effects of "model spectra" in the equations of superconductivity which appears to be necessary if the recently obtained experimental results on La, single crystal and deformed Nb, and Nb_3Sn are to be explained.

III. Artificial Barriers for Superconductive Tunneling

Fabrication of satisfactory tunneling barriers on A15 metal substrates is central to the success of a detailed tunneling investigation of the microscopic superconducting parameters associated with high transition temperature materials. Although the development of suitable barrier fabrication technology is difficult for almost any substrate material, the A15's present a particularly severe challenge. Our approach has been two-fold in its emphasis. We have systematically pursued the more conventional avenues of surface oxidation, and at the same time we have made a significant laboratory commitment to the development of non-substrate oxide (or artificial) tunneling barriers. Such barriers can sometimes be made more rugged, thicker, and more insulative than the natural oxides of a particular material[1] (e.g., rhenium). Examples of kinds of artificial barriers that have been used by researchers are barium stearate layers,[2] thin films of semiconducting materials,[3] and very thin layers of completely oxidized aluminum.[4]

We have focused on amorphous carbon as a promising barrier candidate.[5] Unlike many semiconductor compounds and certain simple elements, carbon is metallurgically well behaved on most substrates of interest. Past experience in our own laboratory[1,5,6] and subsequent efforts in other laboratories[7,8] has shown that 100-300Å layers of amorphous carbon can form usable junction barriers on simple substrate metals such as Cu, Sn and Pb films, on a smooth-surfaced recalcitrant oxidizers such as rhenium single crystals, and on exotic materials such as Nb_2Se.

The goals of our current carbon work are: to determine the effects of film aging, resistivity, fabrication method, substrate cooling during deposition, thickness, and substrate species on observed barrier performance; to determine an optimal approach for barrier fabrication on A15 substrates of interest by establishing the capabilities of carbon barriers on substrates of various personalities, and to apply the technique of amorphous carbon barriers to A15 materials themselves. We have fabricated both arc-evaporated and electron-beam deposited carbon films as cryogenic tunnel barrier layers. In the case of arc-evaporated carbon films extensive investigation of the relation of fabrication to observed electronic properties of isolated carbon films was also made. The study included high temperature annealing treatments and microstructural examination.

(i) Previously Reported Results

Seventy-five isolated films of arc-evaporated carbon were fabricated on room temperature glass substrates at rates varying from 2 Å/sec to 150 Å/sec and pressures varying from 5×10^{-3} Torr to 5×10^{-5} Torr.[9] Final thicknesses of the films ranged from 50 Å to 1600 Å. Resistivity along the length of the films was investigated over the temperature range of 4.2 to 500 K.

Resistivity was independent of deposition rate for films of thicknesses greater than 100 Å and deposited at rates in excess of 10 Å/sec. Typically, resistivity was observed to be about .4 to 4 Ω-cm and could be fabricated with 83% reproducibility for this resistivity range in a moderate vacuum of 5×10^{-5} Torr. Deposition rates slower than 10 Å/sec resulted in a wide

variation in film resistivities, ranging over six orders of magnitude (10^{1} Ω-cm to 10^{7} Ω-cm). Poorer vacuum increased the observed range of variance (10^{-1} Ω-cm to 10^{7} Ω-cm). For a given deposition rate, an order of magnitude increase in vacuum pressure yielded approximately an order of magnitude increase in film resistivity.

For heating temperatures up to 500 K, hysteresis was observed in resistivity-vs-temperature curves for the first few room temperature to room temperature heating/cooling cycles; then it disappeared. Room temperature resistivity dropped approximately a factor of 10 after the first heating/cooling cycle. There is some suggestion in the literature that the hysteresis is the result of a microstructural temperature dependence in the ratio of diamond-like regions to graphite-like regions comprising the film.[10] Since we did not see hysteresis effects for heating/cooling cycles involving cryogenic temperature and room temperature, this suggestion does not seem applicable. We believe that the higher temperature hysteresis effects are more likely due to changes in the background level of conduction-contributing impurities and defects in the carbon films.

Furthermore, the microstructural information we obtained on our samples by TEM showed them to be extraordinarily amorphous: the "as grown" films were structurally disordered (i.e. amorphous) on a scale of 2 Å resolution. Further, the films remained disordered after a heating/cooling cycle. Resistivity, although influenced by impurities as evidenced by the pressure dependence noted, showed no apparent microstructural sensitivity over the temperature range investigated.

(ii) Current Research

An additional twenty-eight carbon films have recently been fabricated by arc-evaporation. These films were sandwiched as tunneling barrier layers between substrate electrodes of In, Al, Au, and Sn thin films and both $Nb_3(AlGe)$ bulk films with counterelectrodes of In, Al, Sn, and PbBi thin films.[11] Data measured along the isolated carbon films discussed above agrees well with measurements done through the sandwiched carbon films. For example, the same wide range of resistivities was also observed through sandwiched carbon layers as along isolated carbon films. The value of 10 Å/sec in deposition rate again appeared as a critical value; the most promising barriers occurred when the deposition rate was of this magnitude. Slower rates gave higher resistivities, sometimes even greater than our tunneling data instrumentation could handle.

Unlike the case of isolated carbon films, the reproducibility of resistivity values of sandwiched carbon films deposited at 10 Å/sec was poor.* The general behavior of these resistivities was to vary inversely with deposition rate. However, the observed behavior of arc-evaporated carbon films cannot be predicted well enough or the arc-evaporation deposition techniques sufficiently controlled to provide the kind of everyday, dependable fabrication technique needed in reasonably large-scale and difficult tunneling experiments such as we are pursuing on A15 superconductors. Therefore, electron-beam deposition, because of its capacity for tighter control of

*The arc-evaporation gun design was probably the cause of this; control of barrier layer thicknesses was erratic.

deposition rate and vacuum pressure, by reducing the heat which causes system outgassing, looked like a better technique.

Thirty-eight sandwich samples of electron-beam deposited carbon films were fabricated in $\lesssim 2.5 \times 10^{-5}$ Torr vacuum; eleven junctions exhibited indentifiable tunneling characteristics of a quality suitable for a detailed superconducting tunneling investigation.[11] Superconducting tunneling structure was unambiguous in the cases of substrate electrodes of indium and tin films (see Fig. 13) and bulk lead-impregnated porous glass (see Fig. 14). Table I summarizes information on these eleven junctions.

Tin substrate junctions were prepared with both arc-evaporated and electron-beam deposited carbon film barriers. Only those junctions fabricated by the electron-beam technique were successful. Figure 13 shows an I-V characteristic for a Sn-C-Sn junction of carbon thickness 100 Å deposited at 11.1 Å/sec. The sum gap, $2\Delta_{Sn}$, is readily visible at a bias of 1.21 mV. The background curvature in the characteristic is commonly seen when junction barrier heights are less than those of natural oxides. Engineering of the barrier height, and thus controlling the degree of curvature-dependent excess current so it does not interfere with phonon deconvolution, is essential.

Activation energies in the carbon were crudely estimated from tangents to $\ln \rho$ vs $\frac{1}{T}$ data on comparably prepared, isolated arc-evaporated films.[9] Typically, these values are 50 mV at room temperature and 3 mV at 5 K, indicating an ill-defined activation energy for such films. $\ln \rho$ vs $T^{-\frac{1}{4}}$ was observed to be linear; in keeping with the amorphous nature of the films.

TABLE I

SUCCESSFUL ELECTRON-BEAM CARBON BARRIERS

Substrate	Counter-Electrode	Carbon Deposition Rate Angstroms/sec	Carbon Thickness Angstroms	Room Temp Junction Resistivity Ohm-cm	Liquid Helium Junction Resistivity Ohm-cm
Indium	Indium	0.9	52	6.25×10^{4}	1.90×10^{7}
Tin	Tin	5.4	130	$<10^{2}$	3.38×10^{8}
Tin	Tin	5.4	130	$<10^{2}$	4.79×10^{9}
Tin	Aluminum	5.4	130	$<10^{2}$	3.65×10^{8}
Tin	Aluminum	5.4	130	$<10^{2}$	3.38×10^{8}
Indium	Tin	11.3	270	$<10^{2}$	2.75×10^{9}
Tin	Tin	11.1	100	$<10^{2}$	4.04×10^{5}
Tin	Tin	11.1	100	$<10^{2}$	1.38×10^{6}
Tin	Tin	11.1	100	$<10^{2}$	5.39×10^{6}
Tin	Indium	11.1	100	$<10^{2}$	1.74×10^{6}
Lead-Impregnated Porous Glass	Aluminum	6.4	95	2.32×10^{7}	1.22×10^{8}

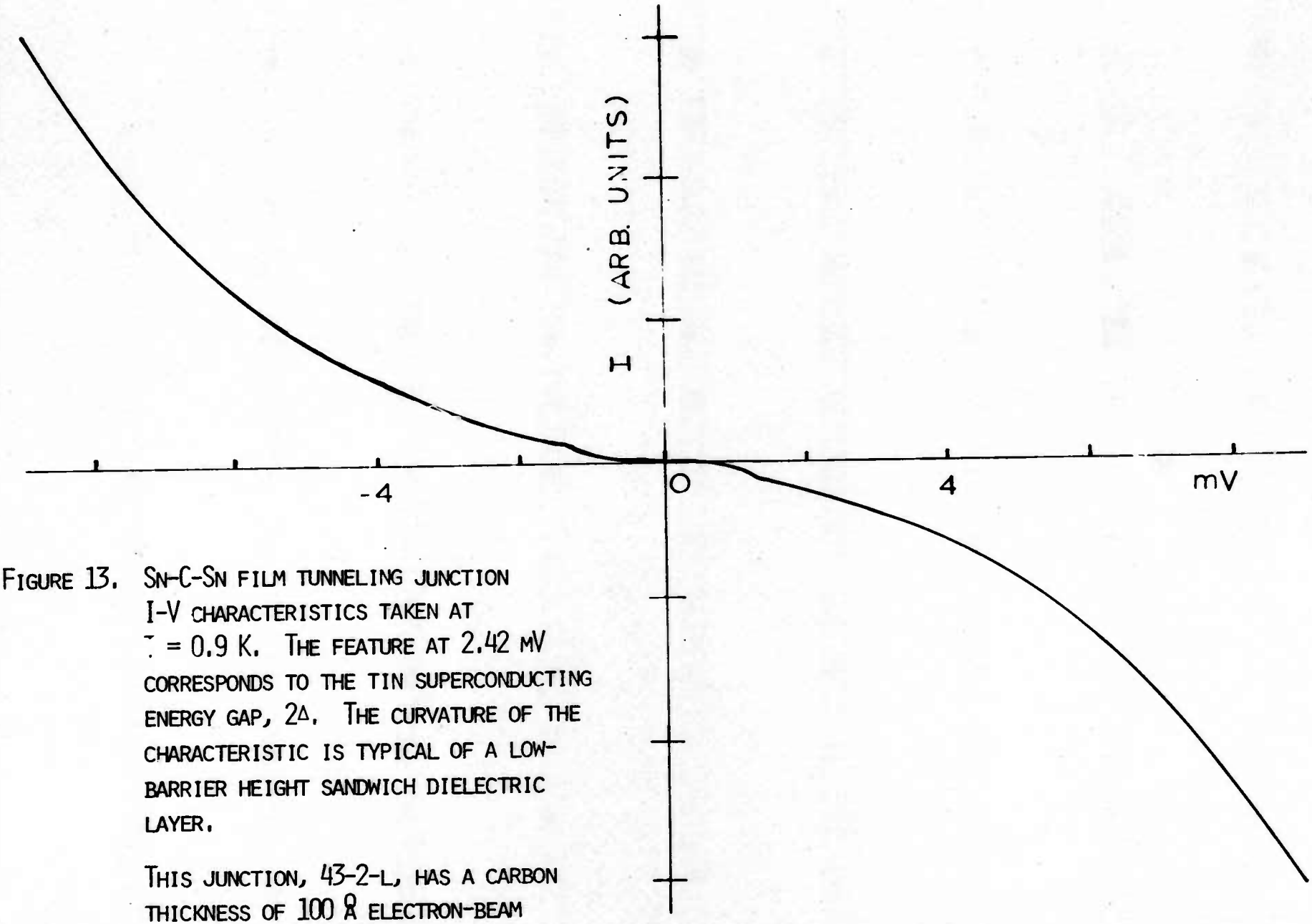

FIGURE 13. SN-C-SN FILM TUNNELING JUNCTION I-V CHARACTERISTICS TAKEN AT $T = 0.9$ K. THE FEATURE AT 2.42 MV CORRESPONDS TO THE TIN SUPERCONDUCTING ENERGY GAP, 2Δ. THE CURVATURE OF THE CHARACTERISTIC IS TYPICAL OF A LOW-BARRIER HEIGHT SANDWICH DIELECTRIC LAYER.

THIS JUNCTION, 43-2-L, HAS A CARBON THICKNESS OF 100 Å ELECTRON-BEAM DEPOSITED AT 11.1 Å/SEC.

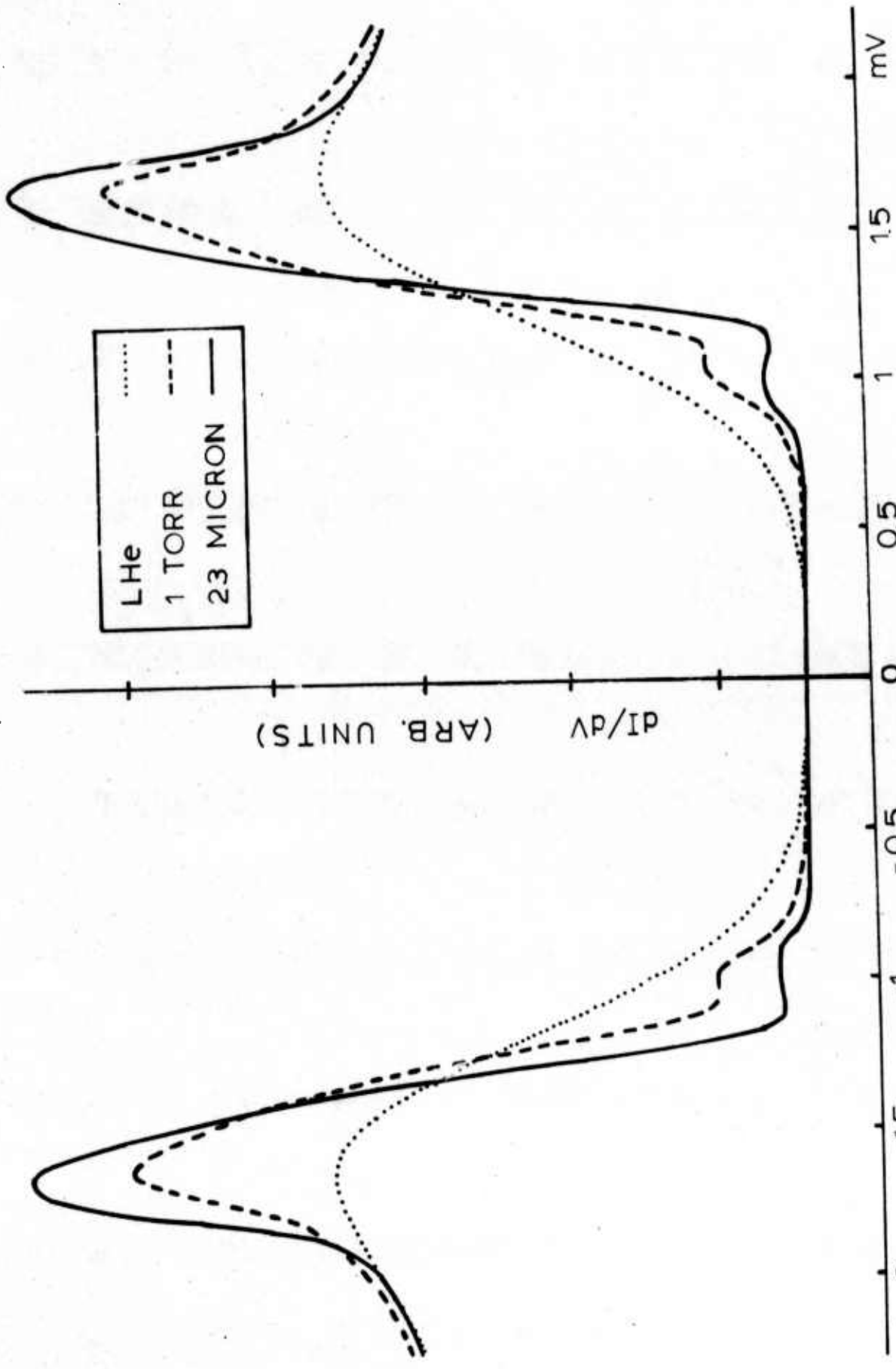

FIGURE 14. DENSITY-OF-STATES CHARACTERISTICS (dI/dV - V) FOR A BULK LEAD-IMPREGNATED VYCOR SUBSTRATE JUNCTION WITH A 95 Å THICK ELECTRON-BEAM DEPOSITED CARBON LAYER AND AN ALUMINUM COUNTERELECTRODE FOR THREE TEMPERATURES: ..... 4.2 K; - - - 1.3 K; AND ——— 0.9 K. THE LEAD-IMPREGNATED SUPERCONDUCTING GLASS

This cryogenic temperature activation energy is a minimum possible value and is of comparable magnitude to superconducting energy gap values. Although this suggests that carbon barrier junctions will never be ideally free of excess currents, this minimum value for the activation energy confirms that carbon can be a viable barrier material. A more quantitative analysis of arc-evaporated carbon of ~100 Å between lead electrodes using Holm's classic barrier model suggests that ~120 mV at helium temperatures is a more realistic value for the activation energy.[7] On the very smooth surface of single crystal niobium and rhenium, we have observed it as high as ~300 mV.[1,6]

Indium substrate junctions were also fabricated using both methods of carbon barrier fabrication. Again, the successful tunneling junctions were those made by electron-beam deposition. One of the successful junctions was even deposited at the extraordinarily slow rate of <1 Å/sec. Success with indium substrate electrodes is particularly encouraging since this material is known for serious agglomeration tendencies which made even natural oxide junction barrier fabrication unusually challenging. $2\Delta_{In}$ was 1.08 mV, in agreement with values reported in the literature.

Bulk lead-impregnated porous glass* is a good test of the carbon barrier technique. Figure 14 shows dI/dV - V for a junction with a 95 Å carbon layer fabricated by the electron-beam technique at 6.3 Å/sec. This is the first planar geometry tunneling data obtained on superconductor-impregnated vycor; previously, only limited success was obtained by the point-contact method and the data resulting was of dubious value for quantitative analysis.[14]

---

*Supplied by Corning Glass Works, Corning, N.Y.

The density-of-states curve is shown at three different temperatures to illustrate the appearance of difference peak, ($\Delta_{glass} - \Delta_{Al}$), as temperature decreased. The energy gap, $2\Delta_{glass}$, is 2.60 mV, slightly smaller, as was expected, than that of bulk lead (2.67 mV). The broad nature of the sum peak located at 1.69 mV, especially on the lower-bias side, suggests that the lead-impregnated vycor is not characterized by a single-gap value, but rather, multiple-gap values. Since the glass-pore size and, thus, the size of the superconducting lead particles is known to vary around an average size of 40 Å, the existence of several gap values is not unexpected. In curves taken out to higher applied biases the phonon structure of the lead was clearly evident.

Tunneling structure was identifiable but accompanied by a major non-tunneling current contributions in junctions of substrate electrodes made of Au films and $Nb_3(AlGe)$ sputtered films and ribbons. The I-V charactertistics of such junctions typically resembled a polarity-independent semiconducting diode or varistor plot. Sucl. behavior has been reported in sputtered carbon layers betwen aluminum film electrodes.[15] These plots indicate a very low barrier height, possible arising from impurities in the barrier itself or from effects of suboxide formation at the metal-carbon interface. The carbon films themselves are electrically continuous and of uniform coverage.

Tunneling structure was not identifiable in junctions fabricated with silver or lead-bismuth film substrate electrodes. Even in these junctions, however, as in all the previously discussed electron-beam deposited carbon layer junctions, the observed properties could be consistently reproduced, in

contrast to the results with arc-evaporated carbon.

Four general criteria for identifying good carbon barrier tunneling junctions have been determined. These concern the color of the carbon film, the deposition rate of the carbon film, the behavior of the slope of the I-V characteristic with temperature, and the junction resistivity at 4.2 K. The criteria do not all have to be simultaneously satisfied; eight of the junctions satisfied some of these criteria; three satisfied all four criteria. Unsuccessful junctions tended to satisfy two or less. It is interesting that all of the criteria relate directly to deposition rate to some degree. This suggests that it is the most crucial fabrication parameter in determining carbon barrier performance.

The visual color of the carbon film is tied to the thickness of the deposited carbon and to the resistivity of the junction. In Figure 15 the outline of the carbon barrier layer is clearly apparent in the sample's crossed-electrode geometry. We have been able to develop a color chart so that for a given deposition rate, the resistivity and final junction performance of such layers can be predicted from their appearance. Films up to 30 Å thick have a clear-to-faint-powdery-white appearance; 30-60 Å films have a nearly invisible, reddish-brown cast to them; around 80 Å, films become distinctly reddish-brown and gradually darken to brownish-black as thickness increases; films in excess of 250 Å are mostly black with a brown cast.

The carbon barriers group according to their resistivity vs temperature behaviors. We can identify several categories of these behaviors, including one where: resistivity typically increases several orders of magnitude

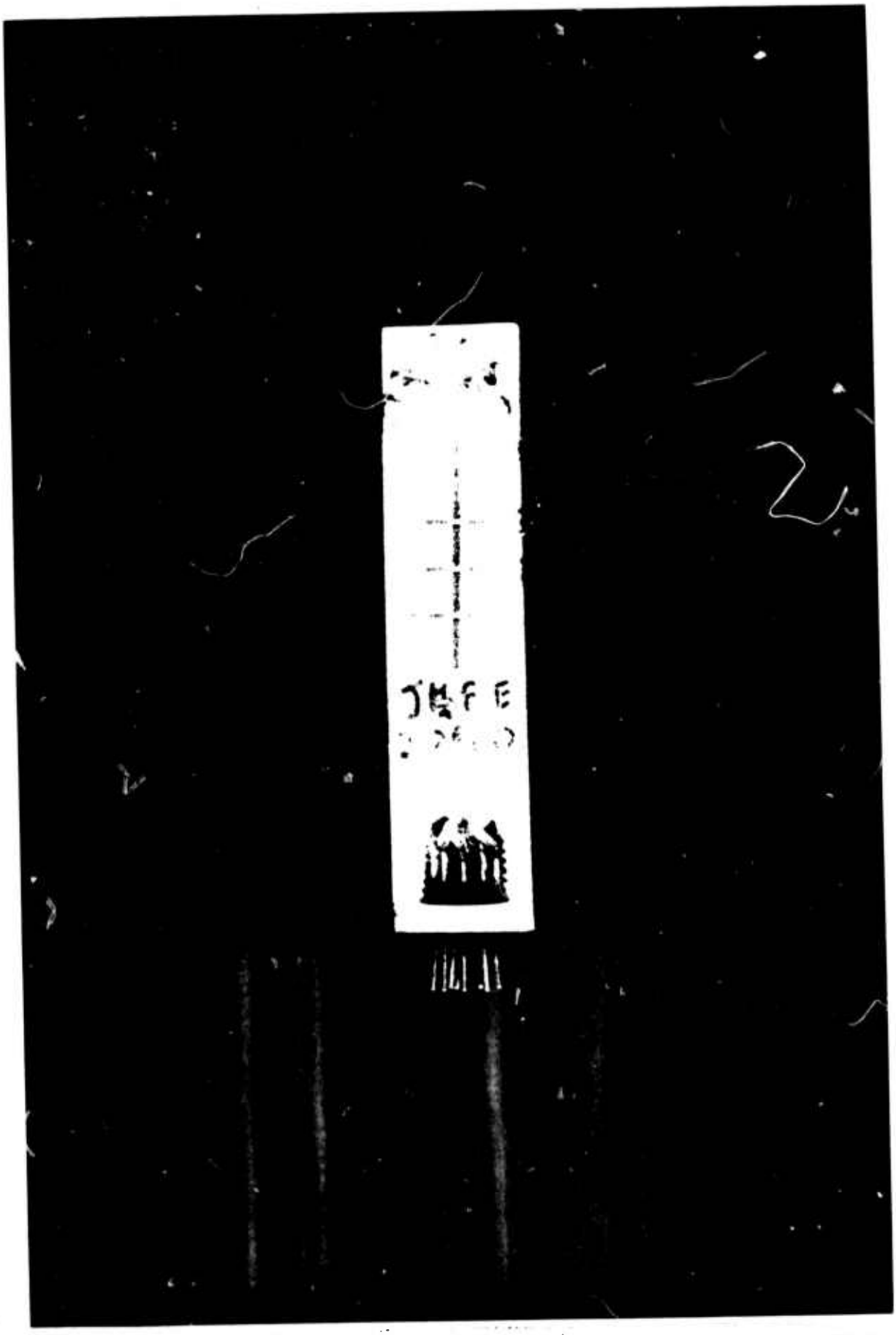

FIGURE 15. CROSSED METAL SUBSTRATE AND COUNTERELECTRODE FILMS SEPARATED BY A WIDER STRIP OF AMORPH CARBON MAKING THREE JUNCTIONS ON THE GLASS SLIDE.

between room temperature and 4.2 K; the deposition rate is approximately 10 Å/sec; and film thickness is generally greater than 100 Å. All eleven of the successful tunnel junctions fall in this category of resistivity vs. temperature, deposition rate, and thickness. For the thiry-four junctions as a whole, resistivity generally varied inversely with deposition rate. For a given rate, resistivity was proportional to films thickness in a non-linear manner.

It was observed that the four-point probe configuration used on the junctions gave negative sloping I-V characteristics at some temperature. Sometimes these persisted well below 77 K before turning positive again in slope. Such behavior is encountered when junction tunneling resistance is of the same order of magnitude as the metal electrode resistance.[13] Reversal of slope sign as temperature decreases is a commonly used indicator of good quality tunneling junctions. Of the eleven successful carbon barrier junctions, nine exhibited this behavior.

As temperature decreased, resistivity increased. For the junction areas used, 4.2 K resistances were in the range of 10 to 7500 ohms, corresponding to liquid helium temperature resistivities of 10^5 to 10^9 Ω-cm, respectively. The literature suggests that good barrier resistance falls between 1-1000 ohms irrespective of barrier material or fabrication technique, and that the optimum oxide barrier resistivity is approximately 10^5 Ω-cm. These carbon barrier junctions are easily as rugged as natural oxide barriers. Repeated temperature cycling did not adversely affect their overall performance. In one respect, however, they tended to behave opposite to oxide barriers:

whereas oxide barriers generally age so as to eliminate tunneling curve substructure related to the barrier nonuniformities or hasten dielectric breakdown; carbon barriers age so as to enhance substructure (e.g., multiparticle peaks) and maintain their dielectric strength.

Another rather intriguing property we sometimes observe in carbon films is a time-rate of change of resistivity under sustained electric field at cryogenic temperatures. In particular, in the sandwich geometry, the carbon layer exhibited continuous changes in resistivity over individual testing periods of approximately one to two hours of applied bias. One manifestation of this change was an increasing smoothing of the superconducting density-of-states as the excess current caused by the changing barrier resistivity began to dominate the signal. There were also other manifestations in the form of structure seemingly related to the barrier itself, not the electrodes. These kinds of behaviors were observed for several electrode species, including bulk $Nb_3(AlGe)$.[16] The effect was distinct from aging, which we also observed. The field-dependent resistivity behavior seems related to a second property sometimes observed in our sandwich geometries. In these cases, over a few minutes or hours and once even over 46 days, the barrier experienced "break-up" under applied bias. The term breakdown refers to the sudden decrease in resistivity of sandwich dielectric layer. In the case of our carbon, the resistivity suddenly increased. Such behavior was observed in different combinations of electrode species.

Recently we have learned of independent observations of similar behaviors by K. Antonowicz[17] who worked with Al-C-Al sandwiches at room temperature. In these samples he observed a slowly decreasing resistivity under applied

bias behavior as we do, and slow time response as well. He observed "break-up" when the resistivity decreased so much as to pass current in excess of a threshold current related to sandwich geometry. The voltages he noted for "break-up" were approximately 2 volts, while our electrode-carbon combinations, tested at cryogenic temperatures, exhibited "break-up" at voltages in the millivolt range. For his voltages, Antonowicz observed that application of a weak magnetic field ($\sim$ ½ gauss) resulted in a sinusoidally varying threshold current, J_{max} vs H. The response time of his junctions was hours. Our junctions were always in the earth's background field; however, our gold substrate carbon barrier junctions did respond to a larger magnetic field with a J_{max} growing and diminishing as a function of increasing field. When we applied fields approximately 10 times larger than the earth's field, we were able to drive some of our junctions out-of, and into, the break-up resistivity mode by consecutive application and turning off, respectively, of the field. Even with no applied field other than the earth's background, we occasionally observed instabilities in the junction's preferred I-V (or resistivity) mode.

Sputtered amorphous carbon films of considerable thickness (1000-3000 Å) have recently been reported by Morisaki, et al., [18] to switch differently at room temperature according to whether the electrodes were aluminum or copper, and according to whether a fabrication configuration was Al-C-Cu or Cu-C-Al. The carbon-aluminum interface was much more definitive in producing Morisaki's switching results than was the carbon-copper interface, the latter often exhibited no switching or memory effects, in fact. His conclusions are in agreement with many of our own observations concerning

the importance of the counterelectrode in the performance of a junction.[19] The vacuum pressure during its deposition, its work function, and its energy upon impact are all known to effect junction performance.[20] Our data further suggest that for both oxide and carbon barriers, effects of the system of substrate electrode-barrier-counterelectrode may be evident in the phonon spectrum we determine from tunneling curves.

Artificial tunneling barriers need not be composed of carbon. An alternative approach is to deposit a thin layer (~20 Å) of a simple metal on top of the substrate material and then to throughly oxidize the layer to form a tough, continuous, insulative oxide. Taylor[4] pioneered this technique utilizing Al and Ti barrier layers. The junctions exhibited reasonable resistances, help up well to temperature recycling and remained stable in characteristics over several days. This barrier fabrication technique has two disadvantages: its usefulness on relatively rough surfaces (such as some of our A15's) is doubtful, and its yield of successful barriers for anyone except Taylor has been almost 0%. On the other hand, no one has been up against a material which is as difficult a substrate as the A15's before, and therefore they did not have to seriously exhaust all barrier fabrication approaches.

We modified our counterelectrode evaporators with stroboscopic shutters in order to be able to control deposition for metal thicknesses of the order of 20 Å. Todate, approximately ten oxidized aluminum layer junctions have been tried on $Nb_3(AlGe)$ and V_3Au arc-cast button external and fractured surfaces. For very thin Al_2O_3 layers (~20 Å), junction I-V characteristics were those of shorts. For very thick aluminum layers (several hundred Å), the characteristics were those of a superconductor-normal junction--indicating

that the aluminum was not oxidized through and that the remaining aluminum was "screening" the effects of the A15 substrate from appearing in the I-V curve. At an intermediate thickness (∿80 Å), definite tunneling structure did occur in the curves consistent with high energy gap values for the A15's. However, the junction characteristics are still far from ideal.

(iii) Directions for Future Work

Preliminary attempts to fabricate bulk V_3Au junctions by formation of an artificial aluminum oxide barrier proved unsuccessful. Subsequent microscopic examination of the V_3Au substrate revealed sufficient surface roughness to account for the barrier fabrication difficulties. Thus we must find new methods to produce a smoother V_3Au surface, but we must also look to a barrier fabrication technique with a tolerance for a rough substrate. Electron-beam evaporated carbon films may be able to fulfill our requirements. We intend to try out such films on vanadium compounds. Based on our experience to date, a carbon layer of ∿100 Å deposited in 10^{-5} Torr vacuum at ∿10 Å/sec should give us our best chance. We have also recently obtained planar geometry sputtered Nb_3Ge films from Westinghouse and from Pennsylvania State University. In addition to pursuing oxide barrier fabrication possibilities, we will attempt carbon barriers on these substrates.

In order to optimize the Al_2O_3 artificial barrier technique and to maintain microstructural integrity across the barrier-substrate interface, we intend to use Nb_3Al as the substrate material. The danger of possible incomplete oxidation of the barrier layer might be offset by the depletion of aluminum

at the alloy surface. We plan to continue to investigate Al_2O_3 barriers on other A15 materials using layers of aluminum of intermediate thickness oxidized in pure heated oxygen or by glow discharge in a partial pressure of oxygen.

We may undertake trial fabrication of barriers on niobium-based alloys [e.g., $Nb_3(AlGe)$, Nb_3Ge] by depositing very thin layers of niobium and oxidizing them through. The better properties of niobium, and the well known oxidation tendencies of this element whenever researchers attempt to sputter it, suggest that niobium oxide layers may be successful barriers on some of our substrate materials.

There are several things that remain to be investigated about the carbon technique itself which should lead to improved tunneling barrier heights:

i) low temperature annealing of the carbon-substrate system <u>in situ</u> before counterelectrode deposition;

ii) cooling of the metal substrate during deposition of the carbon;

iii) deposition of the carbon in the presence of particular gaseous species;

iv) intentional contamination of the substrate metal surface prior to carbon deposition.

IV. Superconducting Microwave Cavities

The goal of this aspect of our research is to develop the technology for the manufacture of practical superconducting microwave cavities. Low losses, high breakdown fields and durable, reliable performance with no degradation, even with exposure to humid air must be achieved before microwave superconductivity will enjoy wider application. The leading candidate material for superconducting cavities is, nominally, pure Nb, for various reasons which are discussed in detail in our previous proposals and publications.[1] However, the development of Nb cavities has been difficult, expensive, and somewhat disappointing in terms of reproducibility of properties, shelf life, and the very elaborate measures needed to produce good properties.[1,2]

Alloys as cavity materials have been relatively speaking, neglected. Several practical reasons for such neglect may be anticipated. Alloys are inherently inhomogeneous: even if the composition lies clearly in a single-phase field on the appropriate equilibrium phase diagram and the possibility of metastable second phases avoided, the phenomenon of coring or non-equilibrium solute segregation is almost completely unavoidable. It is also true that for many alloys the surface is not representative of the bulk,[3] although this need not be true for different alloys under special fabrication conditions. Historically, there was also the belief that H_{C1} would be the limiting AC field for microwave applications[4]; however, recent theoretical[5] and experimental[6] results suggest that the upper limit may be H_C rather H_{C1}.

Since the paractical problems associated with preparing Nb for cavity material seems as great as the problems involved in preparing a good, homogeneous binary substitutional alloy, we reexamined various alloy systems with high transition temperatures for an alternative. We chose to investigate $Mo_{.75}Re_{.25}$ for the following reasons:[7]

(1) it has a high T_c ($\sim$10°K) to allow for low theoretical loss at practical operating temperatures, and a high H_c ($\sim$1600 G);

(2) low κ to give a high H_{c1} ($\sim$500 G) since it had not been conclusively shown that H_c not H_{c1} is the limiting magnetic breakdown field. Furthermore a low κ increases the stability of the low loss Meissner state and should lessen the effect of small inhomogeneities via the proximity effect;

(3) it is a solid solution alloy and therefore eliminates many of the bulk and surface homogeneity problems associated with the compound;

(4) 25 at. %Re gives the highest T_c for the MoRe system without the presence of the normal conducting σ second phase;

(5) solubility for interstitials is a minimum in the MoRe system at 25 at % Re;

(6) MoRe alloys have nearly ideal magnetization curves without the extensive annealing required for similar behavior in Nb;

(7) the thermal conductivity of Mo-25Re is higher than that of Nb at low temperatures which should increase thermal stability at high power levels.

Approximately a year and a half ago we completed the first measurements which demonstrate the feasibility of the Mo-25Re alloy as a superconducting cavity material for microwave application.[1] The measurements were made on TE_{011} mode Nb cavities with removable Mo-25Re backplates. We subsequently showed that these measurements indicated an upper bound of 2.8 microhms for the surface resistance of the backplate at 1.5°K and 11.2 GHz, and a lower bound of 102 gauss for the breakdown field.[8] We believe these figures

to be quite conservative, as it is highly probable that the breakdown occurred in the Nb component, as did the losses due to resistance; in any case, such a surface resistance already corresponds to useful device applications if the breakdown field can be improved. Subsequently, we fabricated two cavities with removable backplates made entirely of Mo-25Re. Initial trials with one cavity after electropolishing and annealing in ultra-high vacuum gave encouraging results, but attempts to optimize surface preparation parameters yielded severely degraded Q-values until these were below our ability to measure them.

(i) Previously Reported Results

In this section we review briefly our initial feasibility study.[1] An electropolished and anodized Nb TE_{011} mode microwave cavity, resonant at 11.2 GHz built from a two piece design in the form of a cylindrical cup and flat circular endplate, was used to measure a $Mo_{.75}Re_{.25}$ sample backplate. The Nb cup and endplate stock were recrystallized at 1400°C in 10^{-8} torr for 2 hours, machined, and electropolished to remove 80μ of surface.[9] Before assembly the cavity pieces were again electropolished to remove 6μ and finally anodized at 20V, 0.5 mA/cm^2 in 12.5% NH_4OH solution. Then they were assembled wet in reagent methanol using In gaskets. The cavity was attached to the wave guide and tested with the single coupling hole always pointing down in order to keep dirt from falling into the cavity. The cavity was evacuated through the waveguide with a liquid N_2 roughing pump followed by a 25ℓ ion pump. The earth's magnetic field was screened to less than 6 mG with μ-metal shielding. The cavity

was measured by means of the decrement method after the Gunn diode microwave source had been passively stabilized to the cavity resonance. The coupling coefficient, β, could be varied by a factor of 30 by means of a movable Nb probe in the waveguide near the coupling hole. A β of 1.6 or less was thus maintained in order to obtain accurate measurements. High power measurements were made with a TWT amplifier and a novel oscillator locking technique which utilized passive stabilization.[1] After initial measurements were made on the all-Nb cavity, the Nb endplate was replaced by one made of Mo-25Re.

The Mo-25Re sample endplate was ground from an arc cast button with a small alumina wheel. The sample plate was then polished by hand with SiC polishing paper and then electropolished with 4:1 methanol to sulfuric acid to remove about 125μm. The final finish though shiny was uneven on a macroscopic scale, particularly at the grain boundaries. Chemical analyses on chips from the sample plate resulted in 900 ppm 0, 2100 ppm C and 40.4 wt.%Re. The rather large amount of 0 and C present was probably due to the arc melting which is a fast melting process and in a large button results in a good deal of trapped gas. Measurements with a susceptability apparatus gave a T_c of 10.1°K. Similar measurements on a much smaller arc melted button resulted in 150 ppm 0, 300 ppm C, 41.3 wt.%Re and a T_c of 9.75°K.

Before assemblage onto the Nb cup, the Mo-25Re endplate was electropolished to remove a further 8μ, then the Nb cup, as well as the backplate, were rinsed in reagent methanol and assembled wet. For an incident power level of 18 mW at 1.4K the Q_o for the all-Nb test was 5.85×10^8 and for the MoRe/Nb

combination 4.50×10^9, yielding a residual surface resistance R_o of 2.8 μ-Ω if the anodized Nb surface can be assumed not to have degraded between tests.* If the Nb surfaces had degraded in any way, R_o for the Mo-25Re would be less, making it even more useful as a cavity material.[1,8] The results of high power tests with the Mo-Re backplate at 1.4K were $Q_o = 1.45 \times 10^8$ at 102 G when breakdown occurred. Although this breakdown probably occurred on the Nb surfaces, it may also be taken as a lower bound for the alloy. A more realistic figure can only be determined in tests with an entire Mo-25Re cavity. It should noted, however, that an increment of a factor of three in this figure would make Mo-25Re as good a cavity as those presently in use in linear accelerator operation.**

(ii) Current Research

Subsequently, in order to obtain quantitative measurements rather than upper and lower bounds, we proceeded to fabricate cavities entirely of Mo-25Re. An ingot with material adequate for two X-band cavities of Mo-25Re was electron-beam melted. After a certain amount of redesign, the first cavity was machined: rough machining was performed by the electrical discharge technique and the final "machining" done by hand grinding. Various trials were carried out on small pieces of the alloy to optimize the electropolishing sequence. A preliminary test was performed on the cavity in the as-ground condition with no heat treatment

---

*In fact, previous testing of the entire Nb cavity indicates this is not so: the cavity always degraded between such tests.[1]

**See Ref. 8 for LINAC parameter estimates.

or electropolishing. The result was an unloaded Q (at 1.4K) of about 10^6, which was encouraging considering the severely disturbed and irregular condition of the ground surfaces. As a test of the relative importance of the severely deformed surface layer (cr ted by the final grinding to shape), we removed 50μ more from the interior of the cavity by electropolishing and then remeasured Q_o which was found to have increased to ca. 10^7 although the cavity was not even on resonance. We estimate that only about half of the disturbed layer had been removed. (No high-temperature annealing had as yet been performed.) A second such test brought the cavity Q to 4×10^7.*

In the first trial of cavity I after a firing anneal at 1800 C in 4×10^{-8} torr pressure a Q_o of 1×10^9 at 1.4K resulted. (This corresponds to a residual surface resistance of 0.7 μ-Ω.) The details of the surface preparations are given in Table (1), entry 4. Before annealing the cavity for this trial, it should be noted, the surfaces resulting from the previous polishing procedures were smooth, bright, and mirror-like except for a few etch pits on the bottom of the cavity. After the heat treatment there were large and visible grains. In addition, during the annealing/assemblage stage the inside of the cavity was accidentally contaminated with diffusion pump oil. An aging test on this cavity showed a Q degradation to $\sim 3 \times 10^8$ after three days; and even cleaning up the pump oil or electropolishing to smooth the surface did not return the cavity Q to 10^9. After this, Q values degraded to very low values even

---

*Most of the tests on the Mo-25Re cavities are low power tests with 10 mW incident power levels.

TABLE 1.

Sequential Surface Preparation -- Cavity I

Test No.	Treatment	Q at ∿ 1.4 K
1.	(As machined) Ultrasonically cleaned; trichlor, acetone, methanol; Rinsed (4 times): methanol.	$\sim 10^6$
2.	Electropolished (11 times) at 27 V using 6:1 methanol/H_2SO_4; Rinsed: H_2O, NH_4OH, then (3 times) methanol.	1.2×10^7
3.	Electropolished 4 times as above; Rinsed: methanol, (2 times) H_2O, then (2 times) methanol.	4.0×10^7
4.[a]	Ultrasonically cleaned as in #1 ; Annealed in rf induction furnance: Cup--Diffusion pump temperature ≤ 1800 C pressure = 4×10^{-8} torr duration = 8 hours cooling time = 23 hours Plate--Ion Pump temperature ≥ 1800 C pressure = 4×10^{-8} torr duration = 5 hours cooling time = 2 hours; Backfill with N_2 gas.	$\sim 1 \times 10^9$
5.	Aged #4 for 3 days.	3×10^8
6.	Degreased: trichlor; Ultrasonically cleaned: methanol; Rinsed (3 times): methanol.	4×10^8
7.[b]	Electropolished 3 times as in #3; Rinsed: H_2O, methanol, H_2O, (2 times) methanol.	3×10^7

TABLE 1. Continued

Test No.	Treatment	Q at ∿1.4 K
8.	Electropolish plate as in #3; Annealed cup/plate in rf furnace with ion pump: temperature ∿ 1550 C pressure = 2 x 10^{-8} Torr duration = 8 hours cooling time = 2 hours; Backfill with N_2 gas.	6.5 x 10^8
9[c]	Aged #8 1 day; Retested in situ (high power).	∿2.8 x 10^8
10.	Electropolish at 19.5 V as in #3: cup--8 times plate--6 times.	1 x 10^8
11[d]	Annealed cup/plate in rf furnace with ion pump: temperature = 1740 C pressure ≈ 4 X 10^{-8} Torr duration = 3 hours cooling time = 16 hours; Backfill with N_2 gas.	2 x 10^7

a. During N_2 backfill, pump oil contamination of surface.

b. A visible bad spot appeared on cavity wall, probably due to arcing.

c. Breakdown field = 74 Gauss.

d. Subsequent treatments $Q \leq 4 \times 10^6$ until cavity remachined.

using very similar surface treatment as described above (see other entries Table 2) indicating that perhaps a drastic change had taken place in the surface composition or that the alloy texture itself had changed because of the various heat-treatments.*

In order to determine if our heat treatments were responsible for the degraded Q's we returned cavity I for remachining. About 70μ of material was removed from the interior surface of the cavity. In the as-received condition there were visible grooves so the cavity was electropolished with a 5:1 solution of methanol and surfuric acid (as in entry 3, Table 1) before testing. Just as before the cavity was remachined, the Q-value was too low to be determined with the present configuration ($\lesssim 10^6$). While this cavity was unavailable our second cavity (cavity II) was received and testing initiated. The results of those trials made us hesitant to reanneal cavity I with our previous heat treatment until we are reasonably sure of the mechanisms operating to degrade our surfaces.

The performance of cavity II has been consistently lower than the best rf values obtained with cavity I. The history of the surface treatments for cavity II are given in Table 2. Initial tests on the as-machined cavity after electropolishing (as in entry 3, Table 1) gave a $Q \sim 6 \times 10^7$ which is a factor of 5 better than for cavity I. This did not surprise us

---

*We calculated the Mo and Re profiles at the surface as a function of annealing temperature to determine the effects of the 1850 C firing. An optimal solution of the Fick diffusion equations (with respect to preferential Mo loss) predicts that an 8 hour 1650 C anneal would result in a decrease of only one at.% Mo at the surface which, of course, should not seriously alter the desired alloy properties. Hence, we lowered our annealing times to be on the safe side.

TABLE 2.

Sequential Treatment: Cavity II

Test No.	History	Q at 1.4 K
1.	(As-machined) Cleaned and Rinsed: Trichlor, acetone, and methanol	$\sim 10^6$
2.	Electropolished to remove 45 μm	6.2×10^7
3.	Anneal at 1650 C for 4 hours (Cooling time = 13 hours)	6×10^7
4.	Electropolish to remove 10 μm Anneal at 1800 C for 8 hours (furnace cool, 14 hours).	$<10^6$

because after this polishing the surface of cavity II looked much smoother and more mirror-like than the same surface for cavity I.* Cavity II was then fired at 1650 C for four hours, wet assembled and measured; Q remained 6×10^7. All subsequent tests, after both additional electropolishing and annealing have had unmeasurable Q's ($<10^6$).

In order to account for these results, several studies have been done on machine chips from the starting ingot, actual cavity surfaces, and on buttons removed from various sections of the starting ingot. We summarize below the various tests and our results.

Chemical Analysis

While the overall composition is close to the Mo-40 wt%Re alloy anticipated, there were indications of small compositional variations through out the ingot.

X-ray Powder Diffraction

The powder pattern for the alloy annealed at 1000 C for 65 hours indicated a pure b.c.c. structure with a lattice constant of 3.1212 Å which is close to the expected value for Mo-25Re. For unannealed samples there were extra unexplained peaks that could have resulted from mechanical strain or oxides.

Electron Probe Microanalysis

This study is inconclusive at the present time but there is a strong indication of the presence of very localized ($\sim$15μ) regions where there

---

*It is true, however, that the visual surface conditions are usually not well correlated to the resulting Q's.

is no Re at all and the Mo content is low in comparison with the matrix. The existence of such regions could easily nucleate the normal regions making the attainment of high Q's all but impossible. The next step in this study is to do a line scan study for the variation in composition on the surface of the various metals used in all aspects of this research (and which could contaminate the surface). Thus, apart from checking the variation of Mo and Re we plan to check for Fe, In, Cu, W, Ta, Nb, and Al, especially Cu.

SEM/EDAX and Photomicrography

These have indicated that, in general, our surfaces for rf tests are smooth. Depending on the type of surface treatment, surface compounds. probably oxides or either Re or Mo, or both, may have been slowly formed on the surface.[10] These could conceivably produce the low Q's we have observed after such treatments. The effects of our heat treatment has been studied by preparing Mo-25Re buttons taken from the starting ingot in the same manner as the actual cavity surfaces. Figure (16a) shows the results (X1,150) of heating at 1850 C (8×10^{-8} Torr) and quench cooling in Argon gas. Subsequent heat treatment, it is felt, might bring up the light "dots" into precipitates. A button heated at 1850 C (10^{-7} Torr) and allowed to furnace cool (x1,150) is shown in Fig. (16b). One of the small diamond shaped precipitates is shown at a larger magnification (x23,200) in Fig. (17a). This sample was then heavily etched in solution 6:2:92 (potassium ferricyanide, potassium hydroxide, water) with results as shown in Fig. (17b) at x5,350. In general, the precipitates are pseudo-acicular in shape, resembling primitive arrowheads, and have a well-defined orientation relative to the crystal structure of the matrix. The appearance of the precipitates in

FIGURE 16. PHOTOMICROGRAPHS OF MO-25RE BUTTONS.

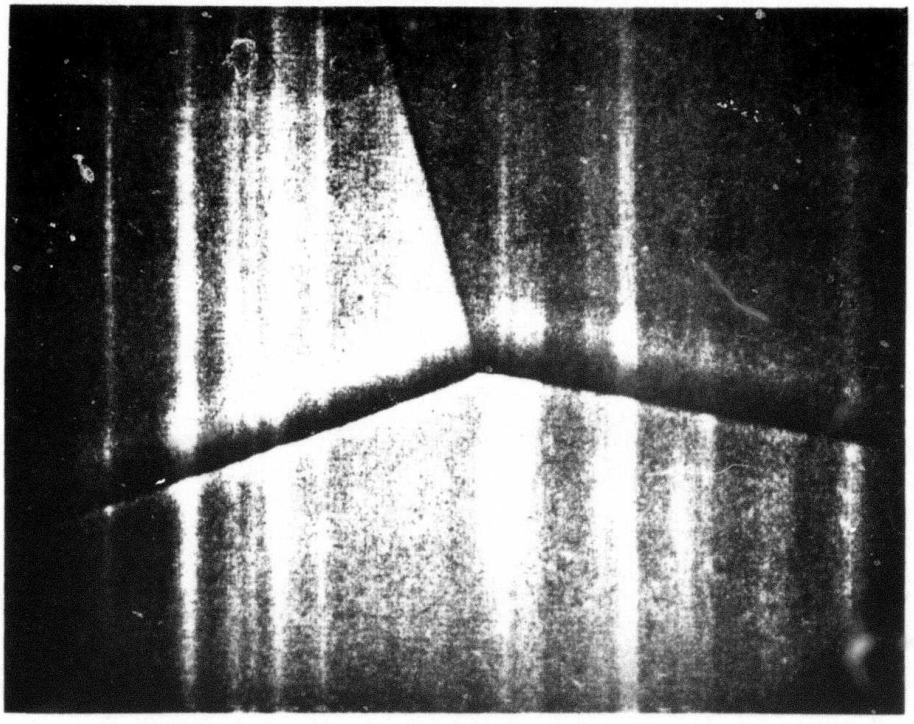

ARGON QUENCH COOLED (x232I)

(A)

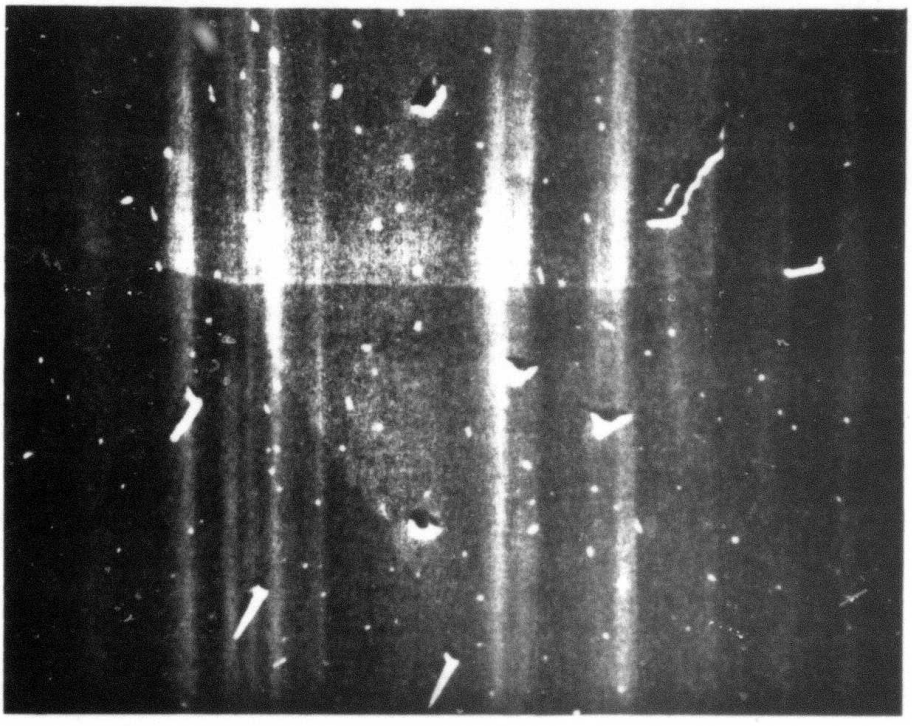

FURNANCE COOLE OVERNIGHT (x11

(B)

FIGURE 17. PHOTOMICROGRAPHS:

(A)

MAGNIFICATION OF A DIAMOND-LIKE STRUCTUR OF FIG. (16B) X23,2000;

(B)

RESULTS OF ACID ETCH (CF. TEXT) ON STRUCTURE IN (A), MAGNIFICATION X5550.

Figs. (16b) and (17a) is due to the section being perpendicular to the preferred acicular axis.

Our preliminary evidence is that these precipitates are alloy oxides. In support of this conjecture, a recent paper[10] on the oxides of foils of Mo_2Re has reported preferential oxidation and evaporation of Mo. In addition, the author points out that the Mo and alloy precipitates form even at low temperatures and on each reheating fresh precipitates have been found. These also have a needle shape although they are not as pronounced as in our study. In our case if we have oxide precipitates, then because the oxides of Mo and Re are both reduced by hydrogen above 800 C, we should be able to "recondition" our srufaces by modifying our tube furnace with flowing H_2 gas.

(iii) Direction of Future Work

The surfaces of our Mo-Re cavities are now being annealed in a hydrogen gas atmosphere at $\sim$ 1000 C. We feel that with the cavities in their present state the hydrogen will reduce the oxides and return our surfaces to their original condition. The first trial with this method made it possible, once again, to measure a Q for cavity I ($\sim 10^7$). Having reconditioned the material, we intend to continue to search for optimal surface preparation techniques. We will then make measurements of the surface resistance and breakdown field as functions of temperature, and investigate othe practical considerations such as conduction aging, "shelf-life", and sensitivity to mere atmospheric exposure. These cavities wil then be used for measurements of basic properties at the alloy surface as a function of surface condition.

V. References

Section II.

1. K. Heckler, G. Horn, G. Otto, and E. Saur, J. Low Temp. Phys. 1 (1969) 29.
2. J. A. Gregory, J. Bostock, M.L.A. MacVicar, and R. M. Rose, Phys. Lett. 46A (1973) 201.
3. James Allen Gregory, S.B. Thesis, MIT (Metallurgy and Materials Science, 1973) unpublished.
4. B. Hillenbrand, H. Martens, H. Pfister, K. Schnitzke, and G. Ziegler, Proc. of 1974 Appl. Supercond. Conf., Illinois IEEE Trans. MAG-11 (1975) 420.
5. ARPA Semi-Annual Technical Report #1, 1 July 1973-31 December 1973,
6. R. Löhberg, T. W. Eager, I. M. Puffer, and R. M. Rose, Appl. Phys. Lett. 22 (1973) 69.
7. J. L. Miles and P. H. Smith, J. Elec. Soc. 110 (1963) 1240.
8. T. P. Sheahan, Phys. Rev. 149 (1966) 368.
9. A. Müller, Z. Naturforsch. 25A (1970) 1659; G. Arrhenius, et al., Proc. Nat. Acad. Sci. 61 (1968) 621.
10. Jeffrey G. Kohr, Ph.D. Thesis, MIT (Metallurgy and Materials Science, 1971) unpublished; C.E. Lundin, A.S. Yamamoto, Trans. AIME 236 (1966) 836.
11. Noah Mendelsohn, S.B. Thesis, MIT (Physics, 1974) unpublished; Myron Hale Frommer, Ph.D. Thesis, MIT (Metallurgy and Materials Science, 1973) unpublished.

12. J. Bostock, Kofi Agyeman, M.H. Frommer, and M.L.A. MacVicar, J. Appl. Phys. 44 (1973) 5567.

13. W. N. Cheung (unpublished).

14. L.E. Hasselberg, M.T. Levinsen, and M.R. Samuelsen, Phys. Rev. B9 (1974) 3757; I. Giaever and H.R. Zeller, Phys. Rev. B1 (1970) 4278; N.R. Werthamer and Sidney Shapiro, Phys. Rev. 164 (1967) 523; N.R. Werthamer, Phys. Rev. 147 (1966) 255.

15. ARPA Semi-Annual Technical Report #1, 1 July 1973-31 December 1973; and Alan Jay Dubin, S.B. Thesis, MIT (Electrical Engineering, 1973) unpublished.

16. W. Hubin, Tech. Rept. 182 (Department of Physics, University of Illinois, Urbana) 1970 (unpublished); W.L. McMillan and J.M. Rowell, Phys. Rev. Lett. 14 (1965) 108.

17. Kuang-Hsin (Ken) Lo, Ph.D. Thesis, MIT (Materials Science and Engineering, 1975) unpublished.

18. R.I. Sharp, J. Phys, C (Sol. St.) 2 (1969) 47 and 431.

19. W.L. McMillan, Phys. Rev. 167 (1968) 331.

Section III.

1. S. I. Ochiai, M.L.A. MacVicar, and R.M. Rose, Solid St. Comm. 8: 1031 (1970).

2. J.L. Miles and H.O. Mahon, J. App. Phys. 32: 1176 (1961); J.L. Miles, S. Shapiro, P.I. Strong, J. Nicol, and P.H. Smith, IBM Journ. 6:34 (1962).

3. I. Giaever, Phys. Rev. Lett. 20: 1286 (1968); I. Giaever and H. Zeller, Phys. Rev. Lett. 21: 1385 (1968).

4. B.N. Taylor, Ph.D. Thesis, Univ. of Pennsylvania (Department of Physics, 1963) unpublished.

5. M.L.A. MacVicar, S.M. Freake, and C.J. Adkins, J. Vac. Sci. Tech. 6: 717 (1969).

6. M.L.A. MacVicar, J. App. Phys. 41: 4765 (1970).

7. Kenji Hatada, M.S. Thesis, Kyushu University (Department of Physics, 1971) unpublished.

8. R.C. Morris and R.V. Coleman, Phys. Lett. 43A: 11 (1973).

9. J. L. Bostock, M.L.A. MacVicar, and R.M. Rose, ARPA Semi-Annual Technical Report #3 (December, 1974).

10. J. Kakinoki, Proc. 5th Conf. Carbon, vol. 2, McMillan Co. (New York, 1963) pp. 499.

11. Keith R. Milkove, S.B. Thesis, MIT (Department of Physics, 1975) unpublished.

12. N.F. Mott, Adv. Phys. 16: 49 (1967); C.J. Adkins, S.M. Freake, and E.M. Hamilton, Phil. Mag. 22: 183 (1970).

13. R.L. Pedersen and F.L. Vernon, Jr., Appl. Phys. Lett. 10: 29 (1967).

14. S.E. Moore and P.P.M. Meincke, J. Appl. Phys. 44: 3734 (1973); R. Soulen, Heat Division, National Bureau of Standards, unpublished.

15. H. Morisaki, H. Iwasaki, and K. Yazawa, App. Phys. Letts. 26: 294 (1975).

16. J.A. Gregory, J. Bostock, M.L.A. MacVicar, and R.M. Rose, Phys. Lett. 46A: 201 (1973); J. Bostock, M.L.A. MacVicar, and R.M. Rose, ARPA Semi-Annual Technical Report #1 (December, 1973).

17. K. Antonowicz, Nature 247: 358 (1974).

18. H. Morisaki, K. Saigo, S. Shintani, and K. Yazawa, J. Noncrystal. Sol. 15: 531 (1974).

19. M.H. Frommer, J.L. Bostock, K. Agyeman, and M.L.A. MacVicar, to be published; K. Lo, N. Cheung, J.L. Bostock, M.L.A. MacVicar, and R.M. Rose, to be published.

20. R.M. Handy, Phys. Rev. 126: 1968 (1962); S.R. Pollack and C.E. Morris, J. Appl. Phys. 35: 1503 (1964); J.C. Fisher and I. Giaever, Phys. Rev. Lett. 5: 464 (1960).

Section IV.

1. John Allen Yasaitis, Ph.D. Thesis, MIT (Metallurgy and Materials Science, 1974) unpublished; and ARPA Semi-Annual Techanical Report #2: 1 Jan. 1974-1June 1974; and references therein.

2. H.A. Schwettman, IEEE Trans NS-18 (1971) 134; J.P. Turneaure, IEEE. Trans. NS-18 (1971) 166; P.B. Wilson, Z. D. Farkas, H. A. Hogg, and E.W. Hoyt, IEEE Trans. NS-20 (1973) 104; and P. Kneisel, O. Stoltz, and J. Halbritter (unpublished).

3. J.A. Gregory, J. Bostock, M.L.A. MacVicar, and R.M. Rose, Phys. Lett. 46A (1973) 201.

4. J.P. Turmeaure, Proc. 8th Int. Conf. on High Energy Accel. (CERN, 1971) p. 51.

5. J. Halbritter, Interne Notiz. No. 130 (1971) Institut für Exp. Kernphysik, Karlsruhe.

6. P. Kneisel, et al., IEEE Trans. NS-20 (1973) 63; and K. Schnitzke, et al., Phys. Lett. 46A (1973) 241.

7. J. Dickinson and L. Richardson, Trans. ASM 51 (1959) 1055; J. Halbritter, Proc. 1972 Appl. Supercon. Conf, Annapolis (IEEE Bulletin) p. 622;

W.C.H. Joiner and R.D. Blaugher, Rev. Mod. Phys., 36 (1964) 67; R.T. Bryant J. Less-Common Met. 4 (1962) 62; D.A. Robins, J. Less-Common Met. 1 (1959) 396; J.H. Brophy, R.M. Rose, and J. Wulff, J. Less-Common Met. 5 (1963) 90; and A.C. Anderson and S.G. O'Hara, J. Low Temp. Phys. 15 (1974) 323.

8. J.A. Yasaitis and R.M. Rose, Appl. Phys. Lett. 25 (1974) 354; and J.A. Yasaitis and R.M. Rose, IEEE Trans. MAG-11 (1975) 434.
9. H. Diepers, O. Schmidt, H. Martens, and F. S. Sun, Phys. Lett. 37A (1971) 139.
10. M. J. Witcomb, J. Less-Common Met. 41 (1975) 45.